Development of Spherical Magnetic Feet and Inverted Locomotion for Multi-legged Steel Structural Inspection Robot

Submitted to
Graduate School of Information Science and Technology
Osaka University

July 2023

Harn SISON

Thesis Committee

Prof. Tatsuhiro Tsuchiya (Osaka University)
Prof. Noriyuki Miura (Osaka University)
Assoc. Prof. Tomohiro Mashita (Osaka University)
Assoc. Prof. Yuki Uranishi (Osaka University)

List of Publications

Peer-Reviewed Journals

1. Sison. H., Ratsamee, P., Higashida, M., Uranishi, Y., Takemura, H. (2022). Generation of Inverted Locomotion Gait for Multi-Legged Robots Using a Spherical Magnet Joint and Adjustable Sleeve. In the Journal of Robotics and Mechatronics Vol.35 No.5. (JRM). (Scheduled Oct. 20, 2023)

2. Ratsamee, P., Hanwong, T., Thungod, K., Sison. H. (2022). A Two-Step Fire Blanket Release Mechanism for Unmanned Aerial Vehicles. In the Journal of Robotics and Mechatronics Vol.35 No.4. (JRM). (Scheduled, 2023)

Peer-Reviewed Conference Proceedings

1. Sison. H., Ratsamee, P., Higashida, M., Mashita, T., Uranishi, Y., Takemura, H. (2021). Spherical Magnetic Joint for Inverted Locomotion of Multi-Legged Robot. *International Conference on Robotics and Automation (ICRA2021)*.

2. Sison. H., Konghuayrob, P., Kaitwanidvilai, S. (2018). A Convolutional Neural Network for Segmentation of Background Texture and Defect on Copper Clad Lamination Surface. *International Conference on Engineering, Applied Sciences, and Technology (ICEAST2018)*.

Domestic Conference Poster Presentation

1. Ratsamee, P., Sison. H., Higashida, M., Uranishi, Y., Takemura, H. (2022). Mechanical Design of Force Adaptive Spherical Magnetic Joint for Inverted Locomotion of Multi-legged Robot. *The 20th Symposium on Construction Robotics in Japan*.

Patents

1. Sison. H., Mashita, T., Ratsamee, P., Uranishi, Y. Walking method of multi-legged robot using permanent magnet. *2021-082695*

Abstract

Steel structure inspection presents significant challenges for robots to operate because the environment is dangerous and hard to access. The objective of this research is to address these challenges using a multi-legged robot, which provides the ability to navigate and traverse the structural environment efficiently by having flexibility from the multi-limb mechanism. However, a challenging area of the steel structure inspection robot is locomotion in an inverted position.

To overcome this challenge, this thesis proposed a Spherical Magnetic Joint (SMJ) with an adjustable sleeve to generate a consistent attractive force for the robot to perform inverted locomotion under steel structures. The spherical permanent magnet allows the robot to attach its foot to a steel surface without energy consumption. Since the robot's inverted locomotion requires foot flexibility for placement and gait construction of the robot. Therefore, the SMJ mechanism was designed and implemented for the robot feet to deal with angular placement. For detaching the foot tip from the steel structure, the adjustable sleeve mechanism assists the robot to control the attractive force by creating a fulcrum point during the tilt and pull step. Experimental results demonstrate that the SMJ can maintain the attractive force at any angle, and the sleeve mechanism can reduce 46% of the presented load during foot detachment compared to direct pulling.

Afterward, the inverted locomotion gaits of a quadruped robot and a hexapod robot, which are the major representative of a multi-legged robot were designed and performed. The SMJ and the adjustable sleeve were integrated on both robots and the detaching step was applied with inverted locomotion of a crawling gait, a trotting gait, a square gait, and a tripod gait. s. Our analysis evaluates the characteristics of each gait in terms of velocity and stability, thereby confirming the versatility of our proposed SMJ, which can be applied to different types of legged robots

Keywords: Steel Structure Inspection Robot, Multi-Legged Robot, Permanent Magnet, Adjustable Sleeve, Inverted Locomotion Gait.

Acknowledgements

In 2018, I entered the Integrated Media Environment Lab (Takemura lab) at Osaka University as a research student and continued to apply as a doctoral course student in a next following semester. I have received a lot of support in many aspects from the lab members. So, I would like to thank the following people for supporting me during my study.

First, I would like to thank my dissertation committee. Prof. Tatsuhiro Tsuchiya, Prof. Noriyuki Miura, Assoc. Prof. Yuki Uranishi and Assoc. Prof. Tomohiro Mashita. Your detailed feedback and advice have been very important to me. Also, my dissertation cannot be done without the committee's comments and review.

I am indebted to my robotic research group leader, Assist. Prof. Photchara Ratsamee for being my guide and encouraging me through the complicated barrier of the robotic field with patience and kindness. I especially appreciate the chance to be a member of the MBZIRC 2020 robotics challenge. I would also like to thank Prof. Haruo Takemura, my supervisor, Assoc. Prof. Manabu Higashida and Assoc. Prof. Jason Orlosky for the valuable comments and advice.

I am also thankful for all present, and past members of Takemura Lab, and friends who have taken their time to help me with the working environment, daily kinds of stuff, and inspiring activities.

Special thanks to DAIKIN INDUSTRIES, Ltd., for the research grant and special researcher position that allow me to access the environment and tools to carry on the experiment in this topic. Also, the Ninety-nine Asian for my scholarship throughout my doctoral years.

Finally, to my parents and my family for all the understanding and generous opportunity to give a chance for me to pursue my dreams and future of robotics.

Harn Sison
Osaka University
July 2023

Contents

List of Tables

List of Figures

Chapter 1

Introduction

1.1 Steel Structural inspection

In several decades, many robotic types of research have been developed for the purpose of helping and assisting human workers to accomplish challenging tasks in our daily life. A steel structural inspection task is one of the tasks that is considered to be dull, dirty, and dangerous circumstances for the workers to explore the area and collect data for inspection of the building condition. Therefore, the steel structure inspection robot [1, 2, 3] became one of the focusing research topics in the robotics field.

So far, several structural inspection robots have been introduced. They were mainly categorized based on the driven mechanism such as wheeled [4, 5, 6], crawler [7, 8, 9] and legged robot [10, 11, 12]. Wheeled and crawler types have the simplest yet most efficient to move around the flat terrain. However, the structural environment consists of beams, bolts, and large gaps that prevent the wheel and belt contact surface to pass through or navigate to different height levels of terrain.

For instance, steel structure plains can be classified into three types. The first type is flat terrain, which is characterized by easy navigability throughout the structure. In terms of mission planning, this type of terrain is often prioritized as the preferred route to avoid obstacles. The second type is rough terrain, which includes areas with small obstacles that do not exceed the height of the robot's wheels or legs.

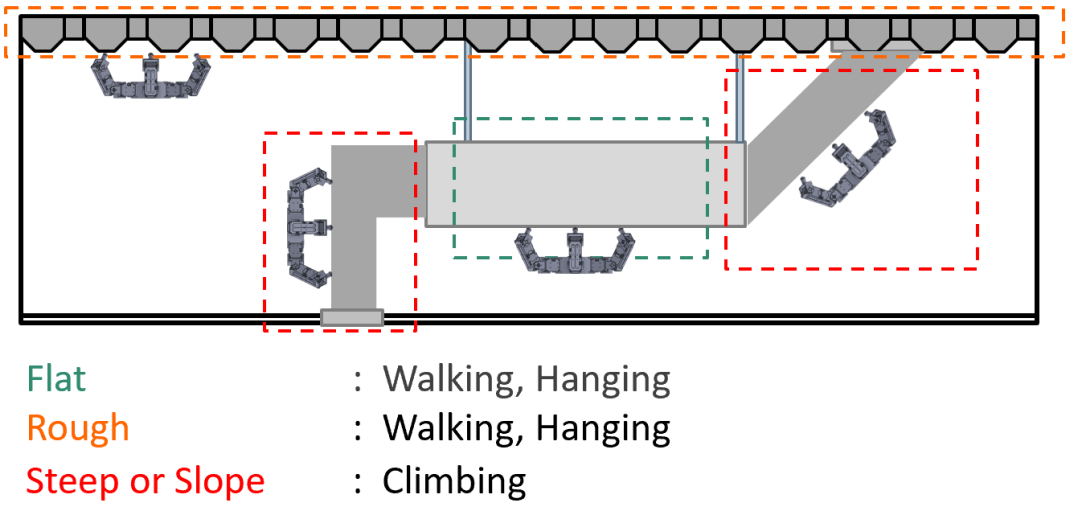

Figure 1.1. Concept of inverted locomotion for multi-legged robot.

The level of difficulty in navigating this type of terrain depends on the type of obstacle, and the robot will opt for this route as a shortcut if no flat terrain is available. Both the flat and rough terrains can be traversed using either ground or inverted locomotion. The third and final type is a steep structure, it will be considered an obstacle if it is difficult to pass depending on the height and the angle. If the robot can pass the obstacle, the robot has to perform climbing locomotion.

Since the legged robot has the ability to step over the obstacle and translate between two different locomotion plain by using the flexibility of the animal's leg anatomy such as limb and joint mechanisms. For these reasons, this thesis will focus on a legged robot solution for the steel structural inspection task.

Moreover, some areas under the steel structure were completely blocked by the obstacle as mentioned. To pass this area, the legged robot requires not only normal locomotion but also inverted locomotion from the structure above the obstacle. Consequently, the adhesion device is required to be developed and integrated with a legged robot. Figure 1.1 shows the perspective of a multi-legged steel structure inspection robot with inverted locomotion.

1.2 Magnetic device for legged robot

The steel structure is mostly built from ferromagnetic substances, which can form an attractive force with the magnetic device. Many magnetic devices such as permanent magnet [13], electro [14], and electro permanent magnet [15] were developed as the adhesion device for the robot depending on the advantages and task of the robot.

The permanent magnet generates the attractive force without energy consumption while the electro-magnetic and electro permanent magnet require the electrical energy to turn on and off the attractive force. However, the maximum attractive force of the magnet depends on the area of contact between the magnet and the ferromagnetic surface referred to in the equation (3.1). This gives the constraint for the foot placing angle between the adhesion devices and the structure surface.

To solve this problem, the author considers a spherical permanent magnet to develop a ball-joint mechanism as a robot end effector for the legged robot (Figure 1.2). This novel mechanism will allow the robot's foot placement to achieve a high degree of freedom for rotational adhesion devices along with the smallest contact area.

1.3 Statement of the Problem

- For creating the walking gait for inverted locomotion, the robot requires to lift the foot before swing to the new position. Because of the always-on attractive force from the spherical permanent magnet, the strong pulling force is generally required to remove the magnet from the surface and might be creating the vibration and cause the robot to fall from the stance. From these reasons, the challenging of developing the spherical permanent magnet joint can be divided in four research question respectively.

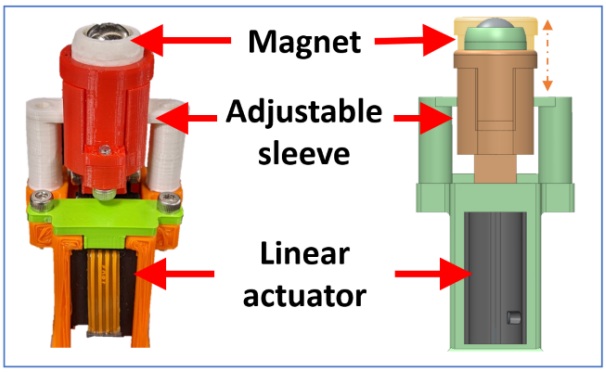

(a)

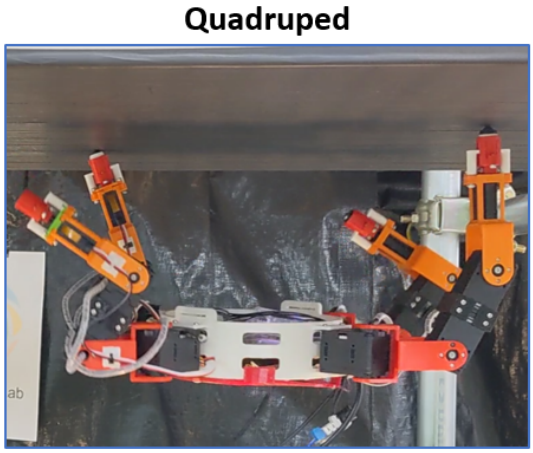

(b)

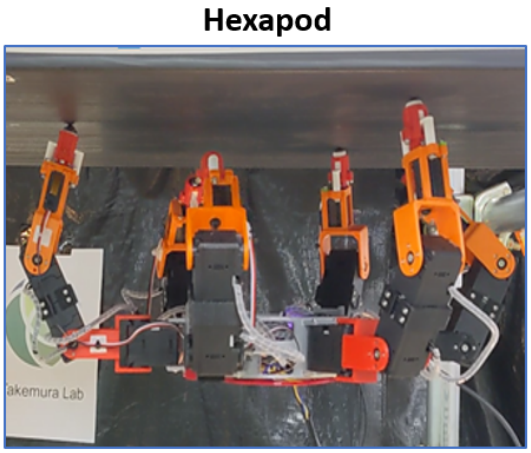

(c)

Figure 1.2. (a) Spherical magnetic joint with an adjustable sleeve. (b) Trotting gait for inverted locomotion of a quadruped robot. (c) Tripod gait for inverted locomotion of a hexapod robot.

1.4 Research Questions

- The first question is, how to design the end effector of the robot's foot with the ability to maintain the attraction force between the magnet and the surface while moving or adjusting the leg position.
- The second question is, how to lift the robot's foot without applying the same amount of attractive force. If the robot applies the direct pulling force to lift the foot, a strong vibration will occur to the robot's body and make the robot fall from the surface.

- The third question is, how to develop the walking gait of the multi-legged robot for the inverted locomotion situation. After the author has finished the design and assembly of the robot's leg, the walking gait for the robot will be designed to deliver the robot from the starting position to the required position without failure. This walking gait should have enough stability and versatility to match the numbers of the robot's leg and the environment's condition.
- The fourth question is, how can the author evaluate the four differences in the walking gait of the quadruped robot and the hexapod robot in the inverted locomotion situation. Each of the gaits requires the evaluation to analyze the advantages and disadvantages of different specifics task of the legged robot.

1.5 Philosophy

Considering the research question from the last section, the author has set up philosophies to answer the research question for pushing the limit in the inverted locomotion of the multi-legged robot. This philosophy consists of four main topics respectively.

First, the flexibility of the foot placing angle must be achieved to support the robot's locomotion. To successfully design the tip of the multi-legged robot's foot, the mechanism must have enough flexibility to break the constraint from the fixed contact angle between the surface and the tip of the robot's foot. Hence, the robot can freely adapt to various walking gaits for traversing through the steel structural building.

Second, the controllability in the attractive force of the spherical magnetic joint has to be developed to avoid the application of the maximum pulling force. Since the vibration and reaction from the direct pulling force cause the robot to fall down. Consequently, the authors must be integrating the legged robot with the assisting device to eliminate or control the pulling force to prevent the reaction from the action force.

Third, the stability of the robot while walking in the inverted locomotion with the different number of the robot leg must be secured since the inverted locomotion has to be performed in different gaits. The legged robot must maintain its stability while walking with minimum support leg to prevent the fall down of the robot or keep moving in the desired direction to successfully perform the task with minimum error.

Fourth, the versatility of the designed mechanism and the walking gait must be verified to adapt the robot's task in various operations. For the real-world application, the developing work requires versatility for the different applications. This will confirm that the author's works have the potential to continue further in this field of research topics.

1.6 Outline of the Dissertation

The overall concept of this dissertation is shown in Figure 1.3. This dissertation consists of five chapters, each of the chapters will be briefly described below.

- ✓ Chapter 1, Introduction, this chapter starts with the background on steel structural inspection robots, Multi-legged robot types, and Magnetic devices. This chapter explains the challenges, research questions, philosophy, and contribution of the proposed method.
- ✓ Chapter 2, Literature Review, this chapter reviews the previous platform of the steel structural inspection robot, the development of the multi-legged robot platform, and the characteristic of the adhesion device.
- ✓ Chapter 3, Spherical Magnetic Joint of Multi-Legged Robot, this chapter shows significant characteristics, design, and experiment results of the spherical permanent magnet and the adjustable sleeve.
- ✓ Chapter 4, Inverted Locomotion of Multi-legged Robot, this chapter explains the design and calculation of the robot platform, the inverted locomotion gait, and the experiment result of the inverted locomotion.

- ✓ Chapter 5, Conclusion, this chapter summarizes the major findings and outlines suggestions for future work.

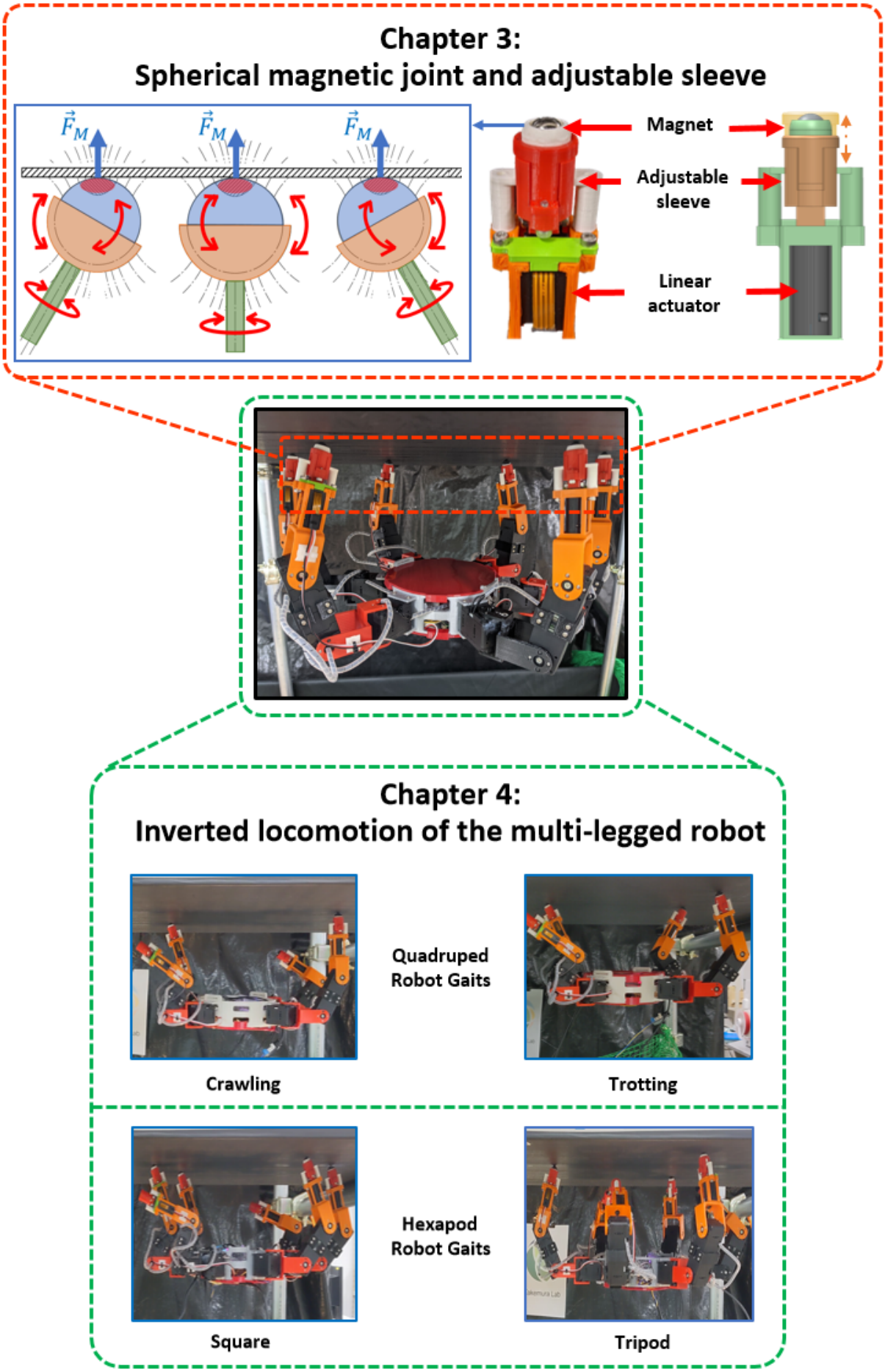

Figure 1.3. Overview of the dissertation

Chapter 2

Literature Review

This chapter presents the related works on three main topics which are important for the development process of this dissertation. There is the steel structural inspection robot, the multi-legged robot, and the adhesion device respectively.

2.1 Steel Structure Inspection Robot

Nowadays, the research and development of steel structural inspection robots has grown rapidly as one of the specific fields of robotics research. So far, several configurations of structure-inspecting robots have been proposed. Based on locomotion type, the robot was classified as wheeled robots, crawler robots, unmanned aerial vehicles (UAVs), and legged robots.

A wheeled type climbing robot in [16] Figure 2.1(a) was developed to inspect the cable in the bridges. The designed robot consists of two spaced modules, connected by the bars and clamps the cable. The main driving system of this robot is wheel contact force and the dc motors. In contrast, the robot in [17] was applied to steel wall inspection with the two permanent magnets wheel for the locomotion of the robot (Figure 2.1(b)).

A crawler-type robot was implemented a track-type contact surfaced to increase the contact force from the large area between the track and the terrain. The steel bridge climbing robot in [18] was applied to steel pipe, flat terrain, and uneven terrain in Figure 2.1(c).

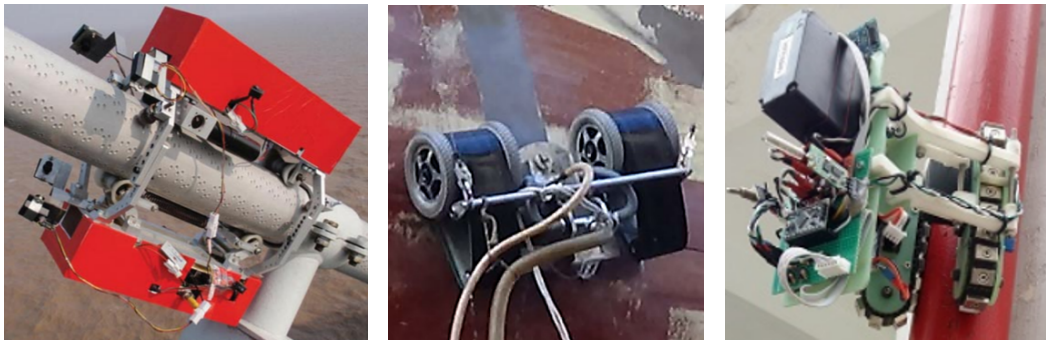

(a) (b) (c)

Figure 2.1. Wheel and crawler type robot. (a) F. Xu. (b) W. Song. (c) S. T. Nguyen and H. M. La.

This robot track system consists of two permanent magnet tracking wheels with the dc motors actuator, the reciprocating mechanism was also integrated to transform the robot to adapt to the different contour surfaces. However, the wheeled and crawler types still have problems when trying to step over large obstacles in a complex environment.

A UAV-type robot was sent to perform a visual inspection in the tall building or avoid the ground obstacle in a complicated design area. This type of robot is floating or flies around the inspection site by using the thrusting force from the rotors and propellers. The aerial structural inspection task in [19] was done by two types of UAV, a rotorcraft and a fixed-wing (Figure 2.2(a)). These two UAVs were implemented with the fast inspection path planning algorithm to execute the inspection in a large opening area for the building. Additionally, the manipulator was integrated into the UAV in research [20], the arm is able to safely touch the structure surface with a sensor while flying, taking measurements from the underside for examples in roof area (Figure 2.2(b)). However, the UAV cannot carry a heavy payload due to its stability during floating or flying. Moreover, a narrow space of the structure will create a strong wind causing a visual occlusion from fog or dust from the environment.

In order to maneuver over a complex area and confined space, the legged robots were presented in multi-dimensional or plane transition contact-type locomotion.

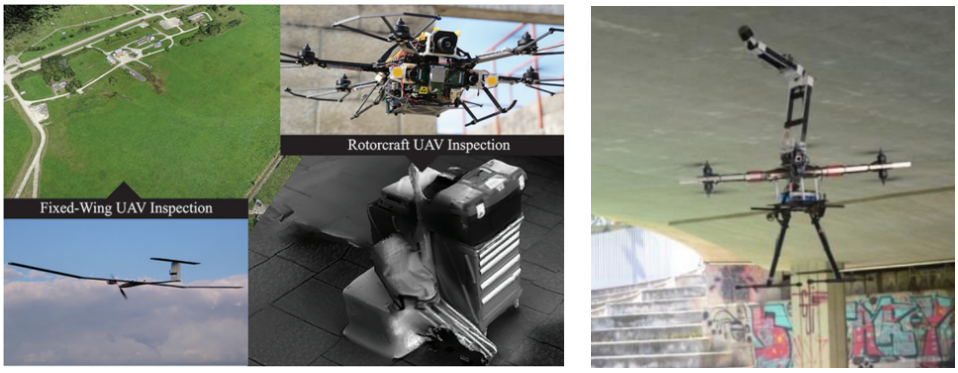

(a) (b)

Figure 2.2. A UAV-type robot. (a) A. Bircher. (b) A. Jimenez-Cano.

2.2 Multi-Legged Robot

The multi-legged robot types imitate the advantages of the animal's leg structure such as mammal, reptilian, insect, or crab. These types of robots have advantages in exploring the structure of buildings, including, flexibility of plane transition, stability during locomotion, and high payload in carrying measuring devices.

A bipedal robot, the human-like robot was developed to inspect and respond to disasters in social infrastructures designed for humans, such as factories and power plants is presented. The humanoid in research [21] was implemented with the new cooling structure to prevent overheat from the CPUs themselves. The robot was successfully climbing the ladder, walking through narrow spaces, and walking over scattered debris as shown in Figure 2.3(a).

A quadruped robot, this robot has four legs configuration, and the robot can be divided into two subcategories. First, a mammal type robot, the ANYmal [22] was developed with a focus on outdoor locomotion such as walking, running, and jumping. Moreover, the full rotation in all joints helps the robot to step over the obstacle or climb the stair (Figure 2.3(b)). Second, sprawling type robot, the leg arrangement of TITAN-XIII in research [23] was placed into this configuration. The sprawling configuration has a wider supporting polygon and lower center of gravity than the mammal type (Figure 2.3(c)). Also, each foot is far enough from the other feet to prevent collision between each other.

(a) (b) (c) (d)

Figure 2.3. A Multi-legged robot type. (a) T. Yoshiike. (b) ANYmal. (c) TITAN-XIII. (d) Weaver.

This robot was developed with a lightweight mechanism. A wire-driven mechanism is used to transmit the power from the motor to the leg for moving with the trotting gait.

A hexapod robot, an insect-inspired type robot, this type of robot imitated the six legs insect to increase the static and dynamic stability of the quadruped robot. A Weaver [24] is the hexapod legged robot that was developed for autonomous navigation on unstructured terrain (Figure 2.3(d)). The adaptation approach uses the unique properties of legged robots by adapting the virtual stiffness, stride frequency, and stride height. As a result, the robot successfully performed and adapt the walking gait autonomously during the locomotion in flat terrain, slope, and multi-levels of an unstructured obstacle.

For these reasons, the proposed research topic is implemented in the steel structure which is classified as the structural environment. Therefore, the multi-legged robot was selected as the robotic platform in this dissertation due to the characteristic of the legged robot type such as carrying high a payload, traversing in multi-dimensional terrain, and climbing the large obstacle.

2.3 Adhesion device

From the previous section, an enormous obstacle can completely prevent the robot to continue the inspection task. Hence, the multi-legged robot requires the potential of performing inverted locomotion. The goal of inverted locomotion is to avoid the ground obstacle by moving in an anti-gravitational situation to cross over the obstacle.

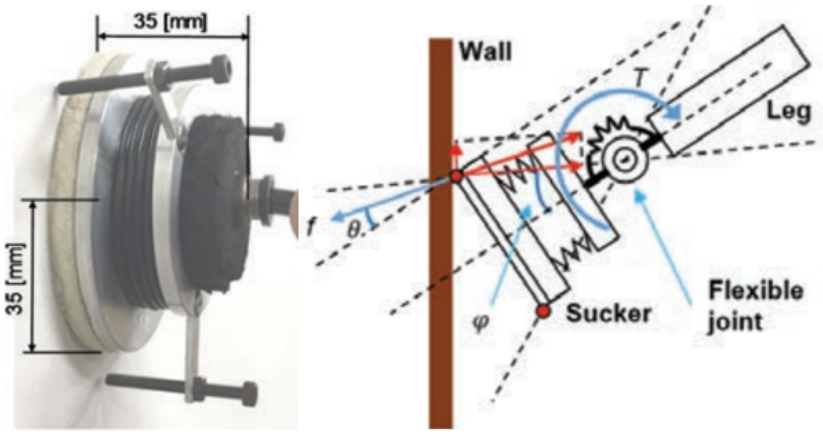

Figure 2.4. Developed sucker and diagram of flexible joint with three point mounting.

To accomplish this, the adhesion device was developed to help the robot to hang itself in the anti-gravitational situation by applying an attractive force between the tip of the robot's leg and the environment surface. Recently, many adhesion devices were developed to assist the multi-legged robot in performing inverted locomotion. The developed tools apply different attractive forces depending on the type of structure and the tools. For glass-type material or smooth surfaces, the vacuum attachment cup is one of the most reliable methods, the multi-legged robot in [25] was integrated with the sucker pad to maintain the attractive force which is generated from the negative air compressor. Additionally, the flexible joint and the three-point mounting were applied to assist the robot for maintain the attractive force in a different situation as shown in Figure 2.4.

As mentioned in the Introduction, the environment of the steel structure was constructed by the ferromagnetic substance which can be applied with the magnetic device. Many of the inspection robots were integrated with magnetic adhesion tools to generate an attractive force with the steel structure.

First, the electromagnets (EM), the attractive force of the EM can be generated by applying a continuous power supply. The electromagnet was implemented in the "ASTERISK [14]" and the "icrawl [26]" in Figure 2.5. These two robots can hang the body in an inverted situation by applying attractive force.

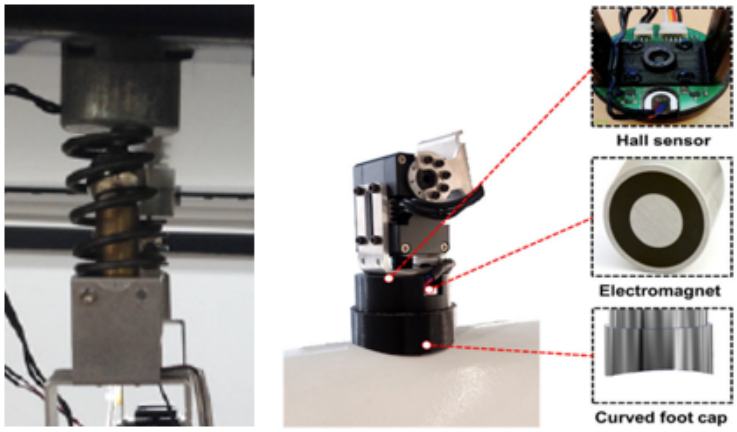

(a) (b)

Figure 2.5. Electromagnet adhesive tool. (a) ASTERISK (b) icrawl

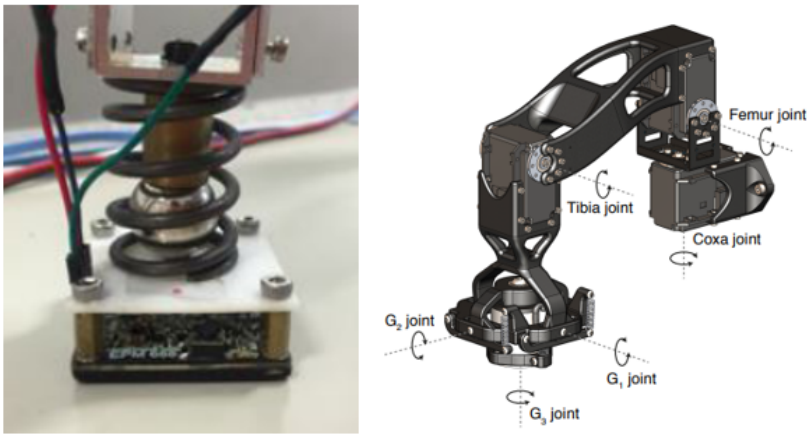

(a) (b)

Figure 2.6. Electro-permanent magnet adhesive tool. (a) ASTERISK (b) Magneto

While performing the locomotion, the EM in the moving leg of the robot is switched off to release the leg from the surfaces.

Second, the electro-permanent magnet (EPM), the attractive force of the EPM was generated from the permanent magnet and does not require the energy to turn on the attractive force. The Magneto [27] and ASTERISK [28] were implemented with the EPM to purpose the concept of the anti-gravitational locomotion Figure 2.6. For the moving leg of the robot during locomotion, the EPM is switched off by applying the power supply to cancel the fixed attractive force.

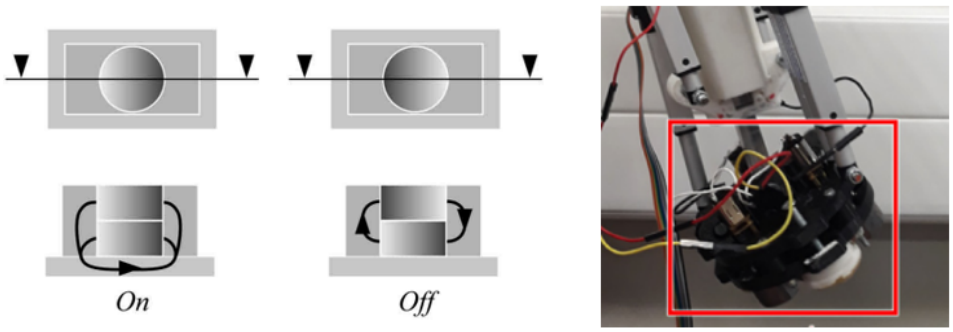

(a) (b)

Figure 2.7. Magnetic switchable device. (a) F. Rochat (b) A. Peidro

Third, the permanent magnet (PM), this device generates a fixed attractive force similar to the EPM. However, the locomotion of the robot requires switching off the attractive force to release the leg of the robot. The Magnetic Switchable Device (MSD) in [29] was presented as a mechanical switching system to turn on and off the attractive force for an application in a climbing robot (Figure 2.7(a)). The inchworm climber in [30] was implemented with the MSD to do the inverted locomotion (Figure 2.7(b)). During the leg lifting step, the attractive force of the MSD in the moving leg is turned off due to the counter magnetic field generated from the control PM.

Additionally, in this research [31] the electro-permanent magnets, magnetorheological elastomers, and ball joint sockets were developed to provide a large adhesion and traction forces, allowing it to walk and climb at different angles. Despite this, every foot tip that is integrated with the square and cylindrical shape magnet requires a fully contracted area to generate a strong adhesive force.

For the proposed robot, the author aims for robust and energy-efficient inverted locomotion. Therefore, the SMJ based on a spherical permanent magnet characterized by its high degree of freedom (DOF) and ability to provide strong adhesive force at a small contact point between the magnet and the surface without energy consumption was proposed. This helps the robot to place its foot with a higher degree of freedom, even on non-flat surfaces.

(a) (b)

Figure 2.8. Magnetic Switchable Device and the MARVEL. (a) Components of the magnetic foot. (b) Quadruped robot MARVEL

Also, to reduce the adhesive force, an adjustable sleeve mechanism at the tip of the robot's foot is proposed. Our experiment result shows that the pulling force is significantly reduced when the adjustable sleeve is activated. Finally, we developed four different gaits: crawling, trotting, square, and tripod gait based on the SMJ for inverted locomotion in both quadruped and hexapod robots, which validates the versatility and robustness of the SMJ on a steel surface with inverted locomotion.

Chapter 3

Spherical Magnetic Joint and Adjustable Sleeve

3.1 Introduction

In this chapter, the author describes a characteristic and design of the Spherical Magnetic Joint (SMJ) and the adjustable sleeve. These two components were applied at the foot tip of the robot for inverted locomotion. The spherical magnetic joint is a tool to generate an attractive force with the flexibility of the ball joint mechanism that allows the foot to be placed at any angle on the surfaces. Additionally, the adjustable sleeve assists the robot to control the force of the tilting and pulling action.

When discussing permanent magnets, an interesting thing to consider is the shape of the magnet and the attractive force. Recently, permanent magnets come in two different contact area shapes, depending on the overall shape of the magnet and the contact surface area. These shapes can be categorized as either flat contact or curved contact. The specific shape of the contact area influences the strength of the attractive force, as a larger contact area yields a higher density of magnetic field, thereby generating a stronger attractive force between the magnets.

However, in our research, the author selected the curved contact type instead of a flat contact type as an adhesive force tool based on the following two criteria: First, our research goal is to design a multi-legged robot with the ability to place its foot to the smallest contact area.

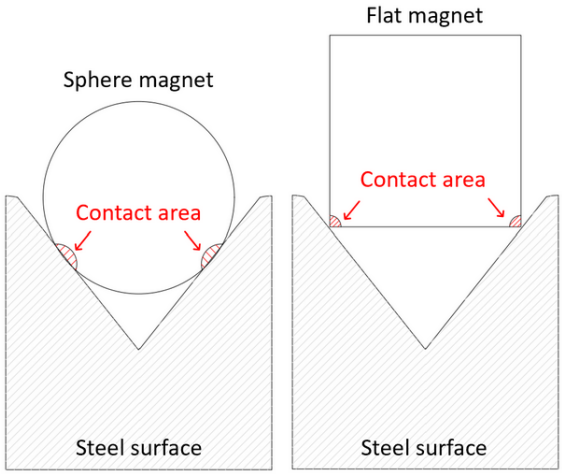

Figure 3.1. Contact surface with curved and flat magnet.

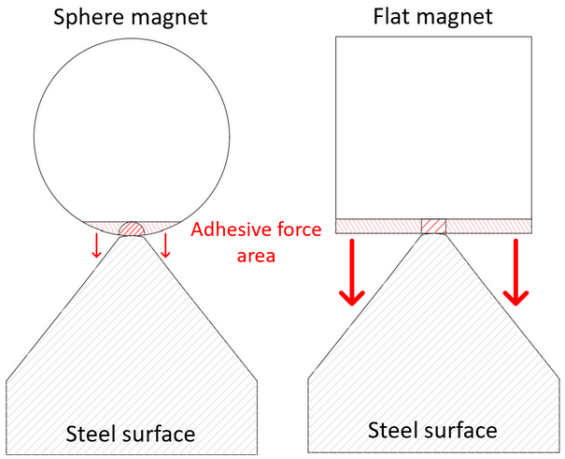

Figure 3.2. Adhesive force of tangential surface between two magnets.

This objective gives our investigation into spherical-shaped magnets, which have a smaller tangential area in comparison to flat contact types like square or cylindrical magnets as shown in Figure 3.1.

Regarding the second criterion, The attractive force generated by the magnet depends on the direction of magnetic flux and the pole position of the magnet. The spherical-shaped magnet can generate the maximum attractive force because the magnetic field always concentrates at the tangential area, while the attractive force of flat contact types may be reduced if they are not placed fully on the surface as shown in Figure 3.2.

The spherical magnetic joint consists of two structures. First, the spherical permanent magnet, this type of magnet has the characteristic of creating a permanent magnetic field to induce the attractive force with the ferromagnetic structure without energy consumption. Also, the permanent magnet shape can be formed in various shapes depending on the user's requirement such as a rectangle bar, circular ring, spherical shape, etc. The author selected the spherical shape permanent magnet for the adhesive tools because the properties of the SPM is suitable in term of giving an attractive force at the small contact area between the surface and the magnet. Second, the ball joint mechanism, this type of connection allows the SPM and the tip of the robot's foot to execute the maximum force due to a free rotational attribute of the mechanism.

However, the foot lifting of the robot requires turning off or decreasing the attractive force as much as possible because the vibration from the pulling force will cause the robot to fall from the hanging situation. The adjustable sleeve was designed to support the pulling action of the robot by setting up the pivot point for tilting the SMJ before lifting. The sleeve design step will be described in the section along with the essential design parameter $\vec{D_R}$. Additionally, the linear actuator was applied as a driven mechanism of the adjustable sleeve to slide and adjust the distance of the sleeve to touch the surface in different situations.

In the experiment, the attractive force of the rotational joint and fixed joint will be compare to demonstrate the advantages of the ball joint mechanism. Also, the three different conditions: direct pulling, pulling where the sleeve radius distance $\vec{D_{R1}}$ = 9.75 mm, and pulling where the sleeve radius distance $\vec{D_{R2}}$ = 8.75 mm will be performed to show the relation of the design parameter $\vec{D_R}$ and the pulling force.

3.2 Spherical Permanent Magnet

In the steel structure climbing and multi-legged robot types, the tip of the foot is required to attach to the surface and have enough flexibility to support the foot at any angle with the surface.

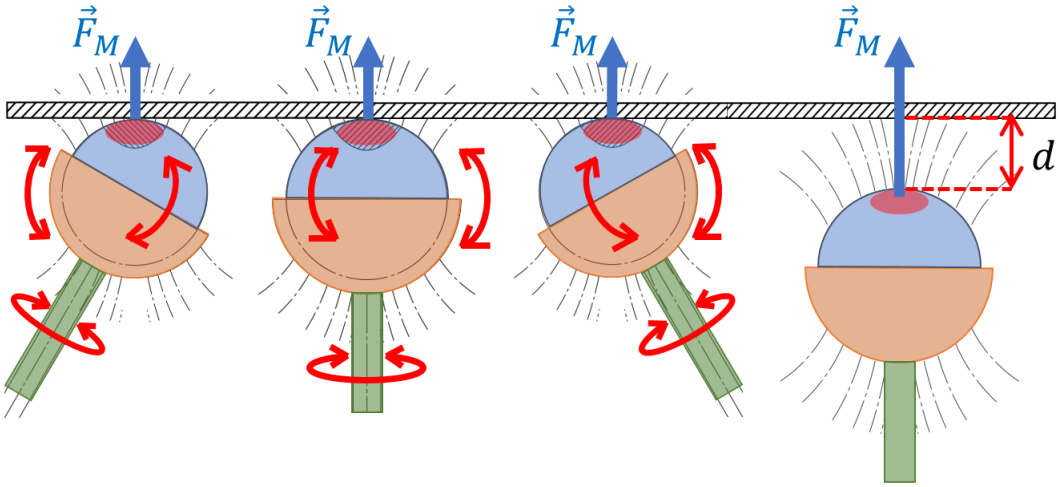

Figure 3.3. Ball joint and spherically shaped permanent magnet. This figure shows the rotation of the ball joint and the characteristics of the attractive force $\vec{F}_M$ of the spherically shaped permanent magnet.

Therefore, the author proposes using a spherical permanent magnet at the tip of the robot's foot on each leg to create an attractive force $\vec{F}_M$.

Characteristic of the spherical permanent magnet is the ability to give the maximum attractive force $\vec{F}_M$ at the small tangent surface of a spherical shape, as in the equation (3.1) :

$$\vec{F}_M = \frac{\vec{B}^2 A_g}{2\mu_0} \tag{3.1}$$

where μ_0 is the permeability $= 4\pi$, $\vec{B}$ is the flux density, and A_g is the coupling surface area. However, the magnetic force $\vec{F}_M$ is decreased when the magnet and the contact surface were separated by the distance as in the following equation.

$$\vec{F}_M = \frac{k}{d^2} \tag{3.2}$$

For the above reason, the coupling area of the magnet is represented at the magnet pole due to the immense magnetic field B, as shown in Figure 3.3.

Considering these properties, the connection between the SPM and the robot's leg must design to support the SPM characteristic. The ball joint mechanism has three rotational degrees of freedom between the two connected components.

The component is free to rotate without preventing the translation in any direction as shown in Figure 3.3. When the magnetic field of SPM is start to apply the attractive force, the pole of the magnet will be rotated toward the surface due to the free rotational condition. As a result, the leg of the robot was allowed to place at any angle while the SMJ applied the maximum attractive force. Also, the connection of the SPM and robot was tested by comparing the rotational and fixed joints. As shown in Figure 3.4, the SPM was implemented within the simple ball joint and fixed joint mechanism. The total attractive force $\sum \vec{F}_M$ of each angle θ was measured by pulling the digital scale until the magnet began to decouple from the surface. Consequently, the spherical magnetic and ball joint mechanisms are suitable for the inverted locomotion of the legged robot. However, the robot is required to turn off the permanent adhesive force during locomotion. Therefore, the next sub-section describes the adjustable sleeve mechanism designed and developed to solve this problem.

3.3 Rotation joint and fixed joint test

As the discussion in the concept of a spherical shape magnet in Section 3A, the connection between the robot legs and the magnet should allow the magnet to maintain maximum force. Because of this, the author designed a simple connection to test the hypothesis of this concept as shown in Figure 3.4. The experiment was conducted by adjusting the angle of link L, θ and pulling a digital scale to measure the $\sum \vec{F}_M$ when the magnet began to detach from the steel surface.

Experiment results was shown in Figure 3.5. The rotation joint gave a consistent force for every θ, while the fixed joint reduced the force due to the area of coupling and the force direction as Figure 3.4. which expected to be $\vec{F}_m \cos\theta$. For this reason, the prototype robot was made with the spherical joint due to the property that it will always make a connection at the pole of the magnet which guarantees a strong contact point with the steel surface.

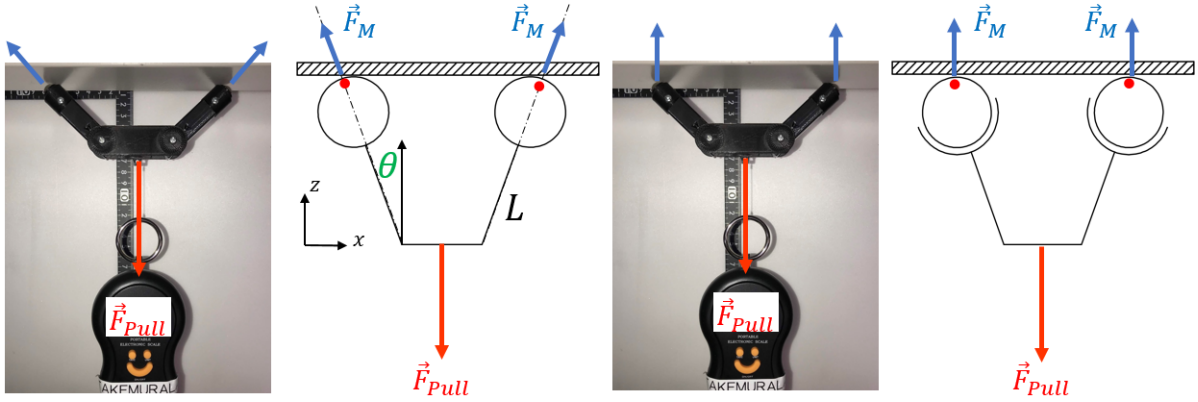

Figure 3.4. Experiment : Simple rotational and fixed joint test concept. Fixed joint (left), Rotational joint (Right)

3.4 Spherical joint and adjustable sleeve

From a concept of the SMJ, we can analyze each of the forces by considering a simple Free-Body Diagram (FBD) as shown in Figure 3.6. To remove the SMJ from the attaching state, the greater direct pulling force $\vec{F}_z$ must be applied in the z-axis (vertical) as shown in the equation (3.3).

$$\vec{F}_z \geqslant \vec{F}_M \tag{3.3}$$

In this case, to remove the strong $\vec{F}_M$, the large and powerful actuator must be integrated to apply the greater $\vec{F}_z$. However, the horizontal force $\vec{F}_x$ pushes a link L to rotate around the SPM because of a smooth surface of a socket. This behavior can be developed into a lever tilting system, a study on [32] introduced the system to tilt a flat permanent magnet-based foot tip without applying the $\vec{F}_z$ which only works on flat surfaces.

Despite the limitations of this method, our research aims to develop a foot tip that can be placed at any angle between the robot's legs and the surface. Therefore, the adjustable sleeve was designed to help the robot detach its legs without using a direct pulling force at a different angle to the placed foot, as shown in Figure 3.7.

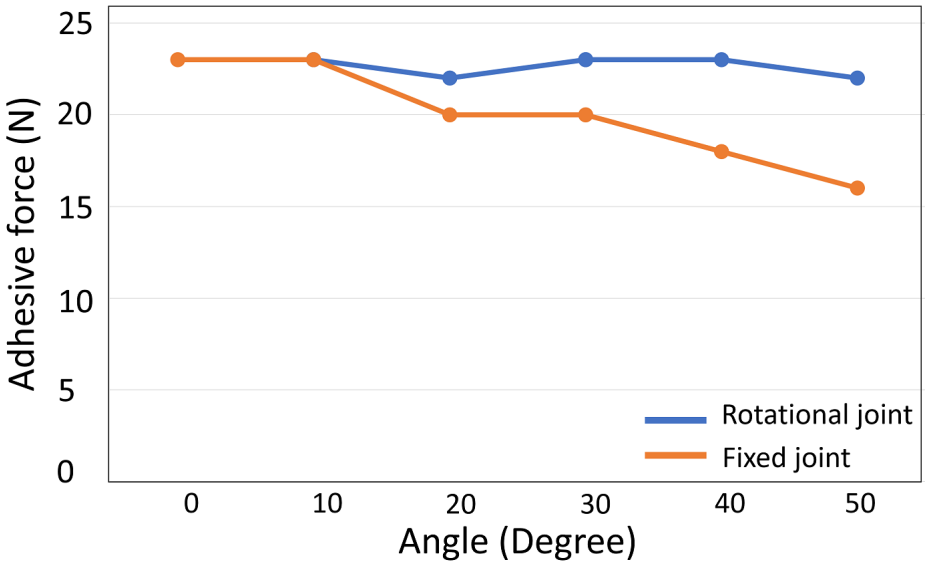

Figure 3.5. Pulling test result. The figure plots a relation between the attractive force of the rotational joint (Blue) and fixed joint (Orange) and the angle of the link.

From the rotational state, a lever-tilting system for the SMJ can be formed by creating the fulcrum point A, from the extended sleeve S as a pivot between the effort and resistance. In this case, the SMJ can be tilted around the point A depending on two conditions as shown in Figure 3.6(b). The first condition is a linear actuator force $\vec{F}_S$ must be greater than the $\vec{F}_M$ to maintain the sleeve position as the rigid pivot point as the equation (3.4).

$$\vec{F}_S \geqslant \vec{F}_M \tag{3.4}$$

The second condition is the static friction $\vec{f}_s$ between the sleeve and the surface must be greater than the $\vec{F}_x$ to prevent slipping during the tilting state as equation (3.5).

$$\vec{f}_s \geqslant \vec{F}_x \tag{3.5}$$

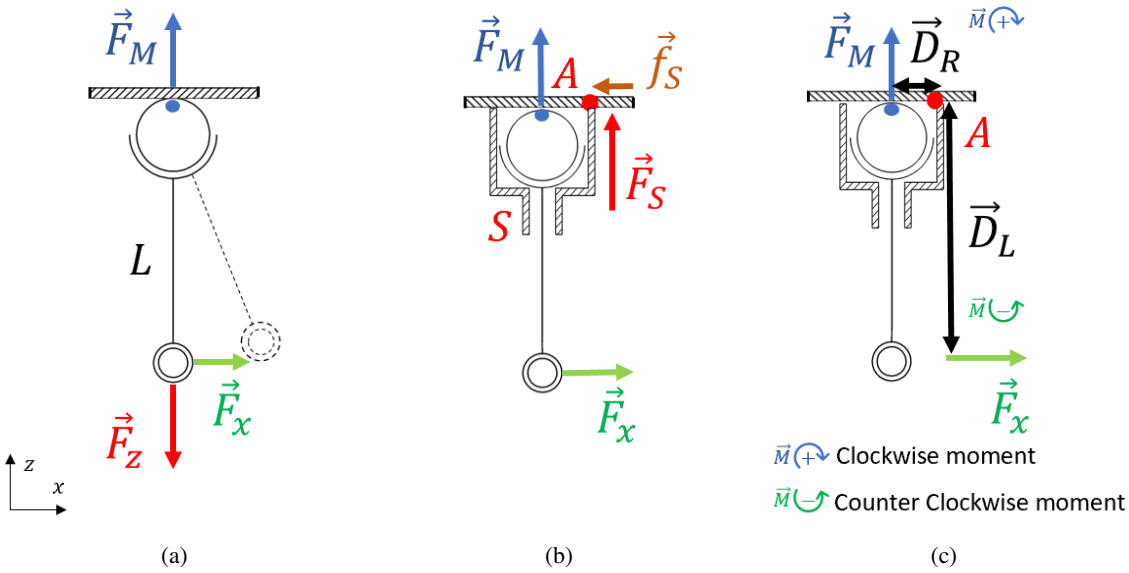

Figure 3.6. Free-body diagrams of each condition of the SMJ: (a) Directly applied force without the adjustable sleeve. (b) Requirement of the adjustable sleeve before tilting the leg. (c) Level tilting force diagram with the adjustable sleeve.

If these conditions were met, we can consider the attractive force $\vec{F_M}$ of the magnet as the resistance and the horizontal force $\vec{F_x}$ from the actuator as the effort. The counterclockwise (CCW) moment $\vec{M}-$ can be derived as

$$\vec{M}- = \vec{F_x} \times \vec{D_L} \tag{3.6}$$

while the clockwise moment (CW) $\vec{M}+$ is defined as

$$\vec{M}+ = \vec{F_M} \times \vec{D_R} \tag{3.7}$$

Where $\vec{D_L}$ and $\vec{D_R}$ is the distance from the $\vec{F_x}$ and the $\vec{F_M}$ to fulcrum point A respectively.

We can tilt the foot around point A by generating the CCW moment $\vec{M}-$ that is greater than the CW moment $\vec{M}+$, as in the equation (3.8)

$$M+ \geqslant M- \tag{3.8}$$

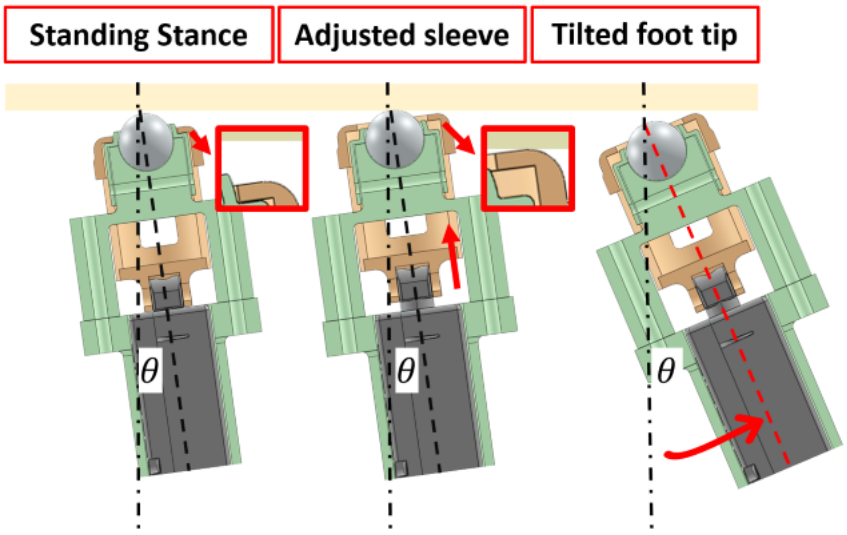

Figure 3.7. Concept of the adjustable sleeve mechanism.

By applying a horizontal force $\vec{F}_x$ through the perpendicular leg L as in the following equation (3.6).

$$\vec{F}_x > \frac{\vec{D}_R}{\vec{D}_L} \times \vec{F}_M \tag{3.9}$$

because the CW moment $\vec{M}+$ from the attractive force $\vec{F}_M$ was created through the sleeve radius distance $\vec{D}_R$ is usually less than the CW moment $\vec{M}+$ and the leg length $\vec{D}_L$, as shown in Figure 3.6(c). As a result, the foot can tilt with the smaller horizontal force $\vec{F}_x$, as in the equation (3.9).

To design the adjustable sleeve, the sleeve radius $\vec{D}_R$ was selected to represent the most important design parameter from the equation (3.9) because the other parameters, such as $\vec{F}_M$, $\vec{D}_L$, and $\vec{F}_x$ were fixed with the robot's overall design and equipment specifications, while the sleeve radius $\vec{D}_R$ can be adjusted to match the structure's surface and the spherical magnet's size. If the sleeve radius $\vec{D}_R$ was designed as small as possible, the horizontal force $\vec{F}_x$ will respectively decrease.

As can be seen from the level-tilting system, the adjustable sleeve is designed to assist the legged robot in tilting its leg during inverted locomotion by reducing the attractive force $\vec{F}_M$ as much as possible.

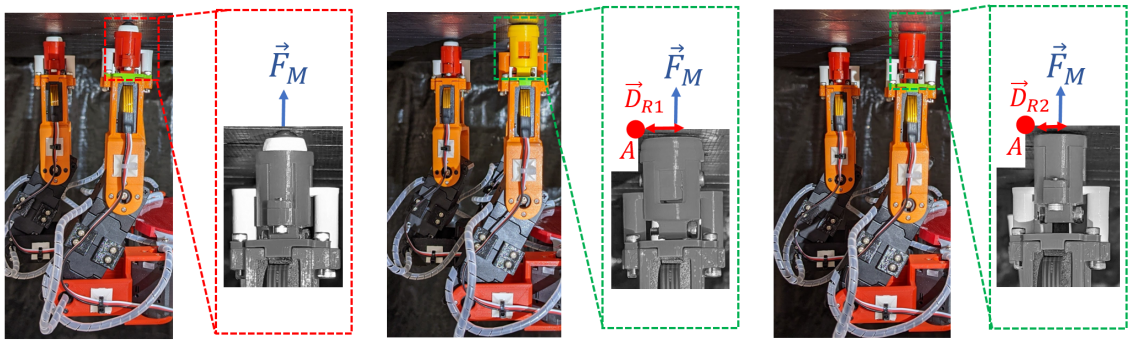

(a) (b) (c)

Figure 3.8. Lever tilting and pulling test: (a) Direct pulling. (b) Leg tilting with $\vec{D_{R1}}$ = 9.75 mm. (c) Leg tilting with $\vec{D_{R2}}$ = 8.75 mm.

Hence, the robot can be equipped with the spherical permanent magnet as the attractive force tool without the problem of controlling the attractive force $\vec{F_M}$.

3.5 Lever tilting and pulling test

This experiment was conducted under three different conditions: pulling, pulling where the sleeve radius distance $\vec{D_{R1}}$ = 9.75 mm, and pulling where the sleeve radius distance $\vec{D_{R2}}$ = 8.75 mm, as shown in Figure 3.8.

Each experiment was conducted 10 times and collected the highest present load data (actual load) of each J_2 actuator. Referring to the XL430-W250-T data sheet [33], the present load can be collected as a percentage of the maximum torque, which is 0.84 N.m. Therefore, we converted the collected data into the unit of torque (N.m) and shown in Figure 3.9.

The result shows that the actuator J_2 present load of pulling without the sleeve (Figure 3.8(a)) reached 0.467 N.m (55%) the highest load among the three conditions. The average present load of pulling with the sleeve $\vec{D_{R1}}$ and $\vec{D_{R2}}$ decreased to 0.13 N.m (16%) and 0.07 N.m (9%) respectively.

This test verified that the adjustable sleeve significantly reduced the attractive force and was able to assist the robot's detaching step by decreasing the horizontal force $\vec{F_x}$ referred to in the equation (3.9).

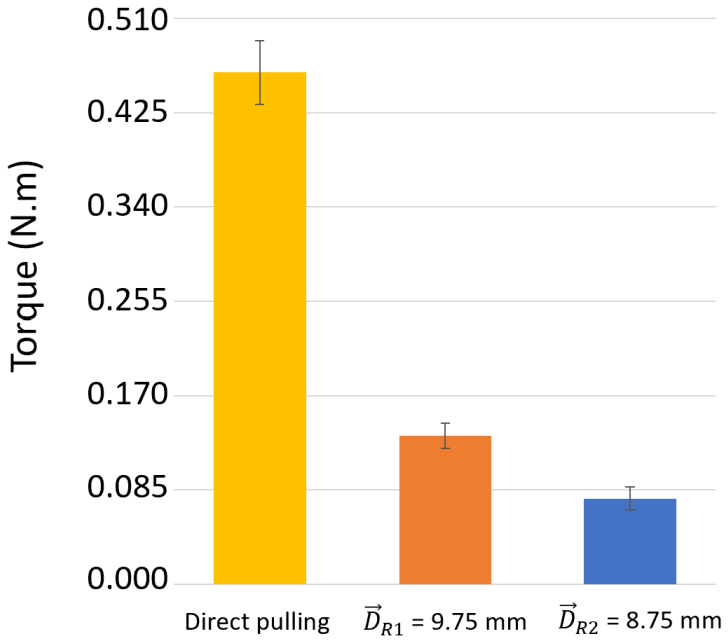

Figure 3.9. Present load result. This figure shows the average result of the highest present load of the actuator J_2 of each pulling and tilting test.

3.6 Electrical power consumption

The next step is to compare how much an electrical power is consumed by the proposed SMJ configuration with the adjustable sleeve and the electro-permanent magnet.

In this experiment, the author set up both the electro-permanent magnet (KEP-3C) [34] configuration and the proposed SMJ configuration with the adjustable sleeve. The power consumption for both of the configurations was measured and calculated following the experimental step. Firstly, the power consumption of the moving actuator was calculated as a reference for both configurations as shown in Figure 3.10. Secondly, the electro-permanent magnet as shown in Figure 3.11. Lastly, the proposed configuration is executed as shown in Figure 3.12, and its power consumption is measured and analyzed as shown in Table 3.1.

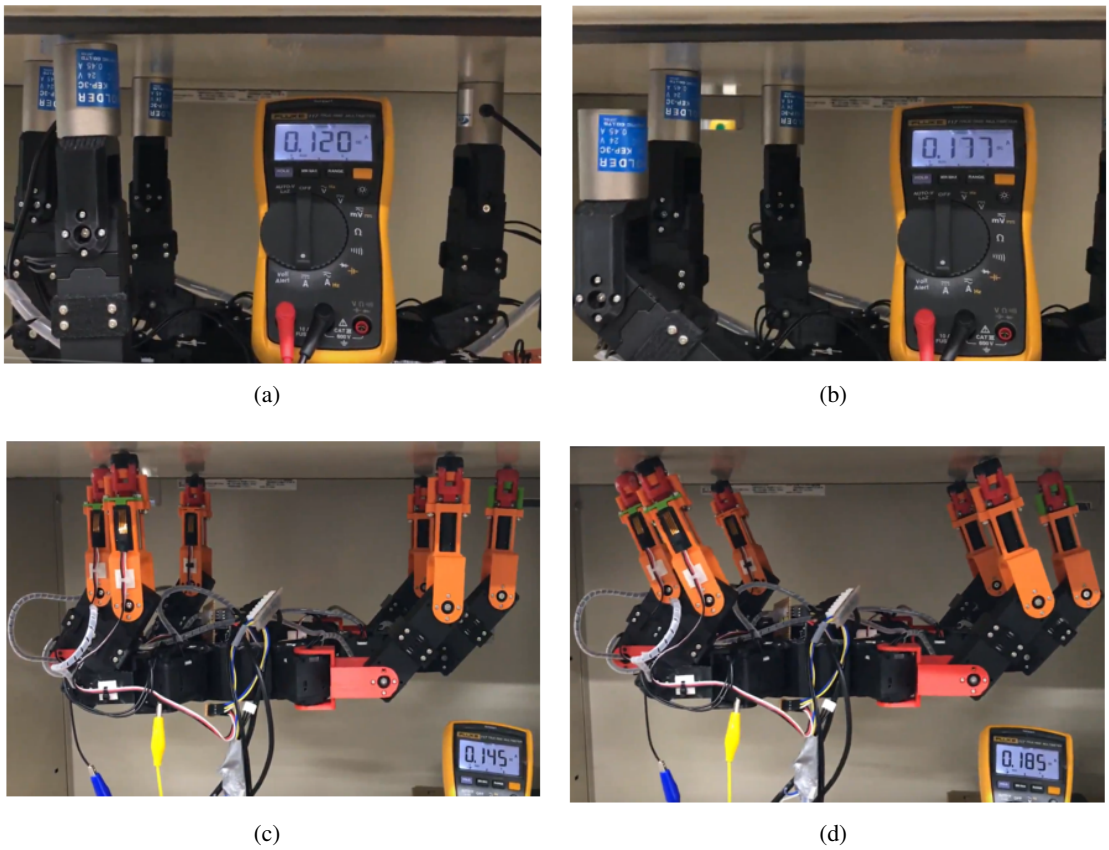

(a) (b)

(c) (d)

Figure 3.10. Current measurement of each configuration. (a) Idle state of actuator with the EPM. (b) Swing state of actuator with the EPM. (c) Idle state of actuator with the proposed mechanism. (d) Swing state of actuator with the proposed mechanism.

3.7 Discussion

The SMJ gave the feet the flexibility to be placed at any angle while the total attractive force $\vec{F_M}$ did not decrease. Also, the adjustable sleeve assisted the tilting of the leg in various detaching steps in gait generation. The smallest sleeve radius distance $\vec{D_{R2}}$ = 8.75 cm, significantly decreased 46% of the horizontal force $\vec{F_x}$ of the tilting foot. However, the unexpected slip during the tilting and pulling with the sleeve occurred due to the friction between the surface, the SPM and the sleeve. The contact area between different materials will give the uncontrollable friction force due to the coefficient of friction, if the friction force is not enough to hold the fulcrum point A, the tilting action will not perform as expected. This will increase the present load in the actuator J_2 (SD = 1.38)

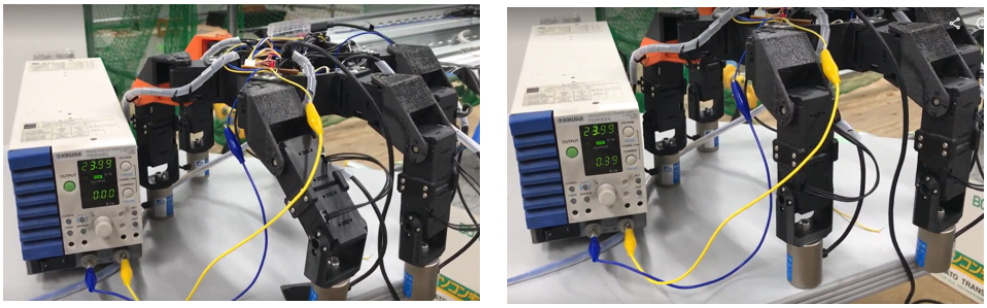

(a) (b)

Figure 3.11. Current measurement of the activating EPM: (a) Activate state. (b) Deactivate state.

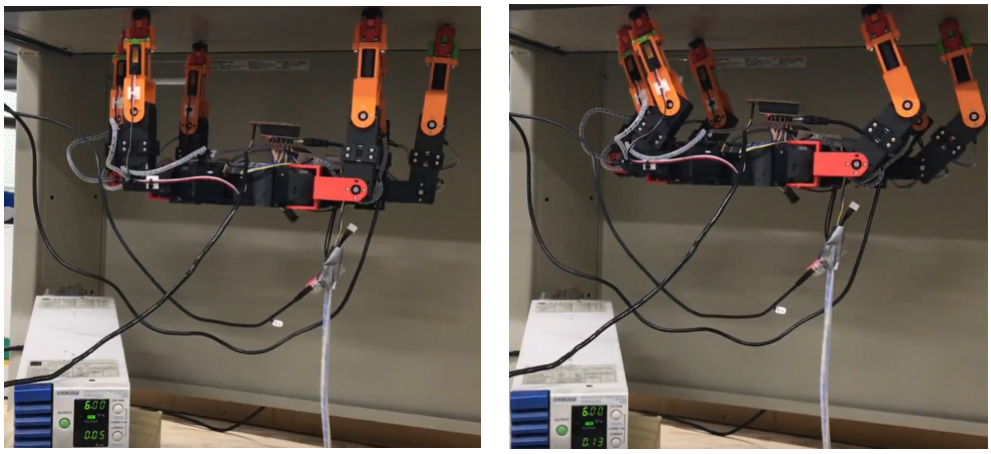

(a) (b)

Figure 3.12. Current measurement of the activating linear actuator: (a) Deactivate state. (b) Activate state.

Additionally, the error of the linear actuator mechanism and the open loop control will decrease the friction force if the sleeve not reached the setting point and create a small gap at the surface. Since the proposed method is indirect control of the permanent magnet attractive force. Consequently, it is understandable that the error cause will be integrated from two different sources: the coefficient of friction from the material and the gap between the sleeve and surface, as the author described.

Table 3.1

Energy consumption

	Voltage(V)	Current(A)	Power(Watt)
Actuator (XL-430-W250)	11.1	0.04	0.45
Electro-permanent magnet	24	0.38	9.12
SMJ with the adjustable sleeve	6	0.2	1.2

3.8 Conclusion

The author proposed a spherical magnetic joint and adjustable sleeve system for a multi-legged robot so that it can perform inverted locomotion. The mechanism allows the robot to place the foot tip at any angle due to the ball joint mechanism's properties and the spherical shape of the magnet. The result of rotational joint and fixed joint experiments showed that the attractive force was equal at every foot tip angle. Additionally, the spherical magnetic joint also provides a high degree of freedom rather than a fully contracting magnet. This higher degree of freedom also helps the robot to walk with a more versatile gait.

The integrated adjustable sleeve system helps the robot deal with leg-pulling action by creating an adjustable fulcrum point to tilt the magnet instead of pulling directly. The experimental result showed that the SMJ with the smallest sleeve radius distance $\vec{D_{R2}} = 0.85$ cm successfully reduced the attractive force from 55% to 9%. Therefore, the low reaction force allows the robot to pull multiple legs to optimize its gait for velocity and stability.

3.9 Contribution

The contributions of the work presented in this chapter were:

- The Spherical Magnetic Joint (SMJ), the proposed adhesive tools and concept is giving flexibility in the multi-angle of the foot placement and stability to maintain the maximum force of the legged robot to successfully perform the inverted locomotion.

- The adjustable sleeve, the assisted mechanism to control the attractive force is allowing the robot to lift the foot without applying the strong pulling force. Hence, the robot is not vibrating or moving during the leg-lifting action.

Chapter 4

The Inverted Locomotion

4.1 Introduction

In this chapter, the author will be explained the multi-legged robot and the gait generation for inverted locomotion. The multi-legged robot platform in this dissertation consists of two different configurations of the robots, which are the quadruped robot and the hexapod robot. The design and calculation of the robot were included in a guideline along with the robot specification. Additionally, the gait generation for inverted locomotion was created to deliver each of the quadruped and hexapod robots from the starting point to the goal point.

The multi-legged robot platform was built to verify the performance of the inverted locomotion that uses the SMJ and the adjustable sleeve for an adhesive tool. A quadruped robot represents a four-legged configuration for agile and simple locomotion of the robot. In contrast, a hexapod robot was constructed with a six-legged configuration by dropping agility to increase the stability of the robot. Furthermore, both of the robot platforms were built with the same material, actuator, and permanent magnet to confirm the versatility of the proposed platform.

In the inverted gait generation, the detaching foot tip will be explained before the gait of quadruped and hexapod robots. The detaching foot tip is focusing on the calculation of the single foot tilting and pulling motion along with an assisting from the adjustable sleeve. Additionally, the full gait generation of each robot was constructed by optimizing the number of detaching legs during the locomotion based on the static stability of the robot.

In the experiment, the performance of four various gaits: the crawling gait, the trotting gait, the square gait, and the tripod gait will be compared in terms of velocity, stability, and accuracy to demonstrate the advantages of each gait.

4.2 Joint stability

In an attempt to build a multi-legged robot, the number of robot legs and the stability of each configuration has to be described. The configuration of robot legs can be divided into three simple configurations: single leg, double legs, and triple legs or more. These conditions will represent the robot's stability in the gait generation section.

4.2.1 Single leg

The first configuration is a single leg, as we can see from Figure 4.1(a), an FBD of the single leg shows that we have fully imitated the SMJ characteristics. The leg can be rotated 360 degrees on a vertical axis (z-axis) and tilted related to the other two axes (x and y) as far as the socket allows. Hence, the single leg is unstable if the external force was applied related to each of the axes.

4.2.2 Double legs

The second configuration is double legs if one leg was added as shown in Figure 4.1(b). This configuration was allowed to be tilted related to only one axis which is the center line of the robot body (horizontal). Thus, the two legs configuration will prevent the 360 degrees rotation along the vertical axis z and the y axes. For these reasons, the robot is unstable only if the external force is applied perpendicular to the center line of the robot.

4.2.3 Triple legs or more

The third configuration is triple legs or more, the FBD of this configuration in Figure 4.1(c) shows that the three legs create a red triangle area which is a support polygon.

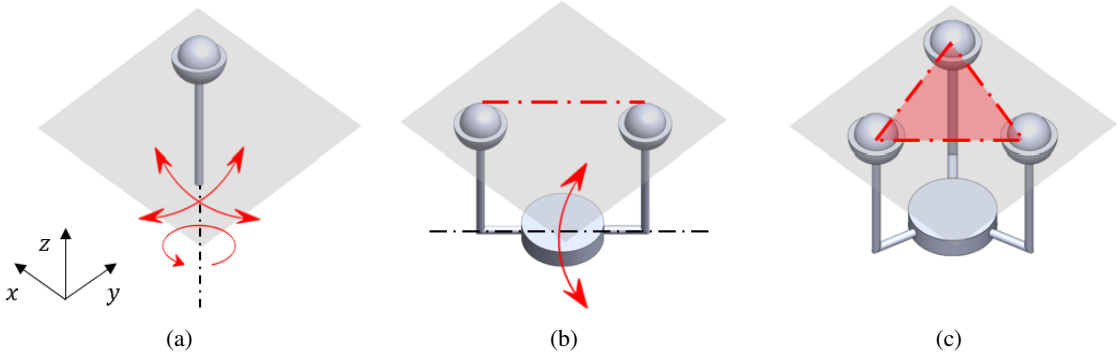

Figure 4.1. Stability of leg configuration: (a) Single leg. (b) Double legs. (c) Triple legs or more.

Any configuration that has fixed corners of the polygon is defined as a static stability system because there are no rotational axes. For this reason, the system resisted to applied force in any direction.

In the following section, we explain the design of the multi-legged robot platform after selecting the spherical permanent magnet and the adjustable sleeve as the anti-gravitational mechanisms for the inverted locomotion of the robot.

4.3 Robot platform

This section presents the multi-legged robot platform, which is used to validate the concept of the steel-structure inspection robot that uses a permanent magnet for an adhesive force along with inverted locomotion to maneuver under the steel structure.

Quadruped robots and hexapod robots were selected as representatives of the multi-legged platform, which covers a majority of designs and locomotion types of multi-legged robots. The differences between these robots are their number of legs and leg arrangement. The robot body was made by a 3-D printer with polylactic acid plastic (PLA) material.

4.3.1 Inverted locomotion robot design guideline

The main concern in designing the inverted multi-legged robot is that the attractive force of the robot must allow it to hang in a sufficiently stable posture.

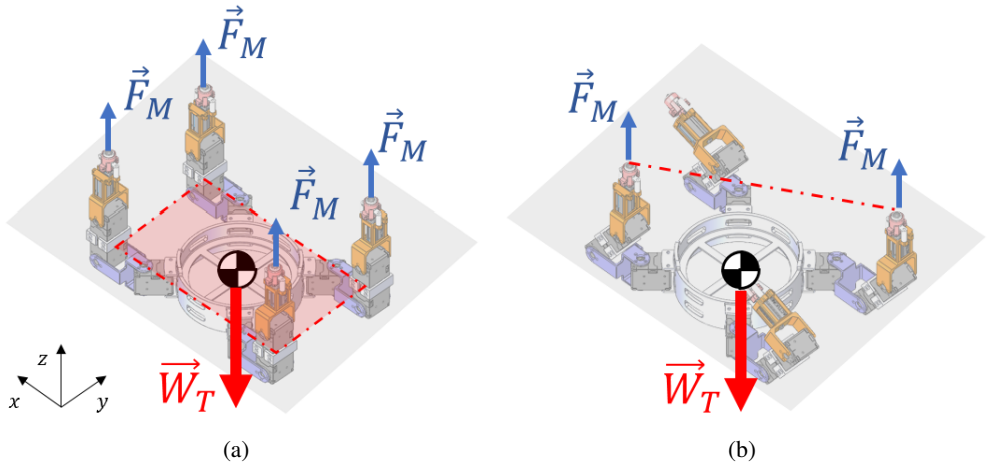

Figure 4.2. Static equilibrium of the robot in each posture: (a) Initial posture. (b) Detaching step.

This attractive force $\vec{F}_M$ must be greater than the total weight of the robot $\vec{W}_T$ as shown in Figure 4.2 to keep the robot inverted under the steel structure.

We expect the magnet of the robot with leg number N to generate attractive force $\vec{F}_M$ on each leg. Accordingly, a static equilibrium that represents a fully attached leg of the robot used in this research is shown in Figure 4.2(a). However, a detaching step during inverted locomotion requires the robot to detach its legs, as shown in Figure 4.2(b), but the total weight is not changed. Thus, the design parameters required a safety factor SF as in the equation (4.1), to maintain the static stability of the robot during inverted locomotion.

$$\sum_{n=1}^{N} \vec{F}_M^n \geqslant \vec{W}_T SF \tag{4.1}$$

From the above equation, we can properly select the spherical permanent magnet as the attractive force $\vec{F}_M$ to be used with the SMJ for the multi-legged robot.

4.3.2 Center of Mass and Force distribution

After the proper $\vec{F}_M$ and the magnet were designed, a force applied for each of the robot legs has to be calculated to find the relationship between the position of the COM (Center Of Mass) and the force applied to each foot.

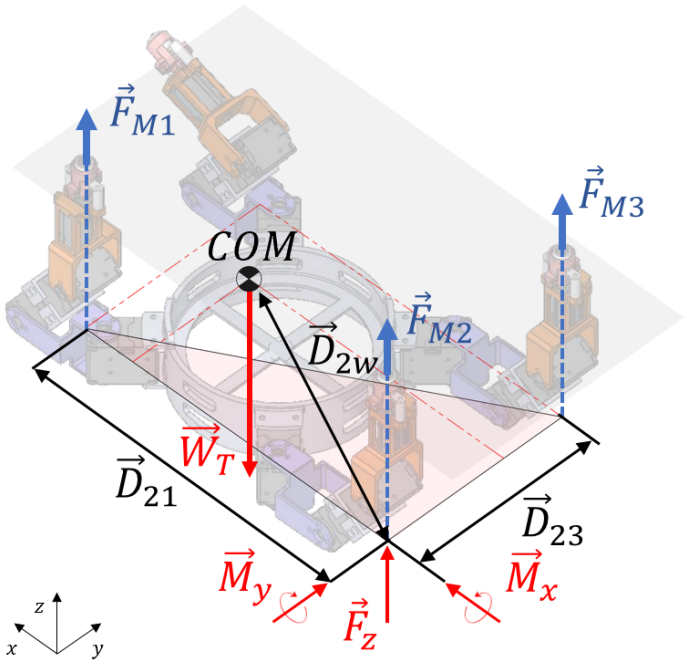

Figure 4.3. Three dimension equilibrium for the multi-legged robot.

In this research, we used three attached legs to represent the relationship because this number can form the significant support polygon and other legs can be counted as redundant legs as shown in Figure 4.3. From a three dimensional, if a fulcrum point was determined on a plane x,y at the $\vec{F_{M_2}}$ we can apply the three equations below and all summation of forces and moments related to each axis ($\sum\vec{F_z}$, $\sum\vec{M_x}$, and $\sum\vec{M_y}$) is equal to 0.

$$\sum\vec{F_z} = \vec{F_{M1}} + \vec{F_{M2}} + \vec{F_{M3}} - \vec{W_T} \tag{4.2}$$

$$\sum\vec{M_x} = (\vec{F_{M1}} \times \vec{D_{21}}) + (\vec{W_T} \times \vec{D_{2w}}) \tag{4.3}$$

$$\sum\vec{M_y} = (\vec{F_{M_3}} \times \vec{D_{23}}) + (\vec{W_T} \times \vec{D_{2w}}) \tag{4.4}$$

where $\sum\vec{F_z}$ is a summation of all forces in z axis, $\sum\vec{M_x}$ and $\sum\vec{M_y}$ are summation of all moments around x and y axis, $\vec{F_{M_1}}$, $\vec{F_{M_2}}$, $\vec{F_{M_3}}$ are force at each of robot's leg, $\vec{D_{2w}}$, $\vec{D_{21}}$, $\vec{D_{23}}$ are distance from fulcrum point $\vec{F_{M_2}}$ to each of the components and $\vec{W_T}$ is the total weight of the robot.

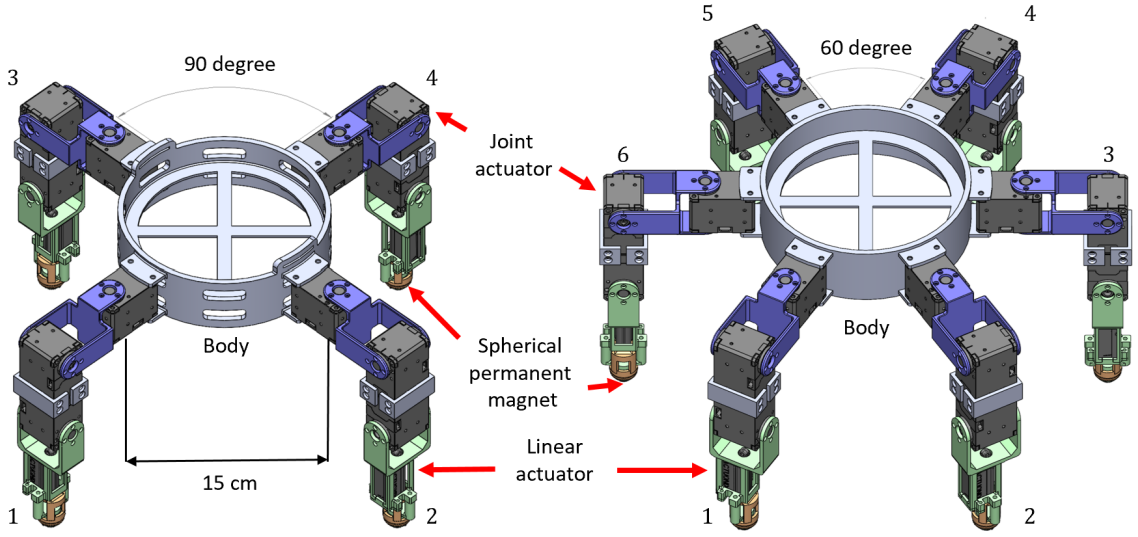

Figure 4.4. Multi-legged robot platform. (a) Quadruped robot. (b) Hexapod robot.

As we can see, the $\vec{F_M}$ will be changed respect to $\vec{D_{2w}}$ as in the equation (4.3) and the equation (4.4). If the COM moves away from the fulcrum point, the moment from $\vec{W_T}$ will increase. As a result, each of $\vec{F_M}$ has to increase to keep the robot in equilibrium.

4.3.3 Quadruped robot

Table 4.1

Robot specifications

	Quadruped robot	Hexapod robot	Unit
Joint Actuator	12	18	Joint
Linear Actuator	4	6	Axis
Spherical permanent magnet	4	6	Ball
Leg	4	6	Legs
Body	1	1	Body
Weight	1.26	1.78	Kilograms
Size	70	70	Centimeters

The quadruped robot type was inspired by the leg arrangement of mammals and reptiles that usually perform static and dynamic gaits. The quadruped robot contains a main body and four legs. The main body is a circular shape and the legs are arranged symmetrically at a 90-degree angle around the body.

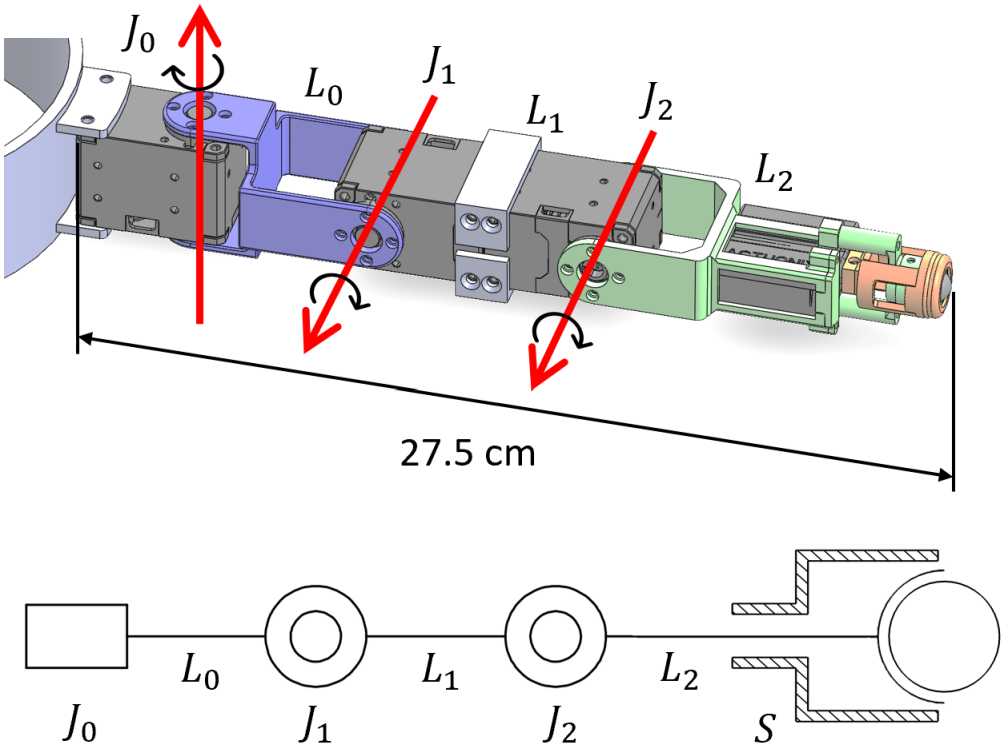

Figure 4.5. The robot leg. This figure shows the components, annotations, and free body diagram of the robot leg.

The total weight of this robot is 1.26 kilograms and the maximum diameter is 70 centimeters from the tip of the far left foot to the tip of the far right foot. Figure 4.4, Table 4.1 and 4.2 show the concept and the components of the robot.

4.3.4 Hexapod robot

In the hexapod robot, the leg arrangement of this robot imitates insect and crab features rather than those of mammals and reptiles. This robot's main body is the same as the quadruped robot but the leg arrangement and number of legs are different. The legs are symmetrically arranged around the robot at a 60-degree angle. The total weight of this robot is 1.78 kilograms and the maximum diameter is 70 centimeters from the tip of the far left foot to the tip of the far right foot. Figure 4.4, Table 4.1 and 4.2 show the concept and components of the robot.

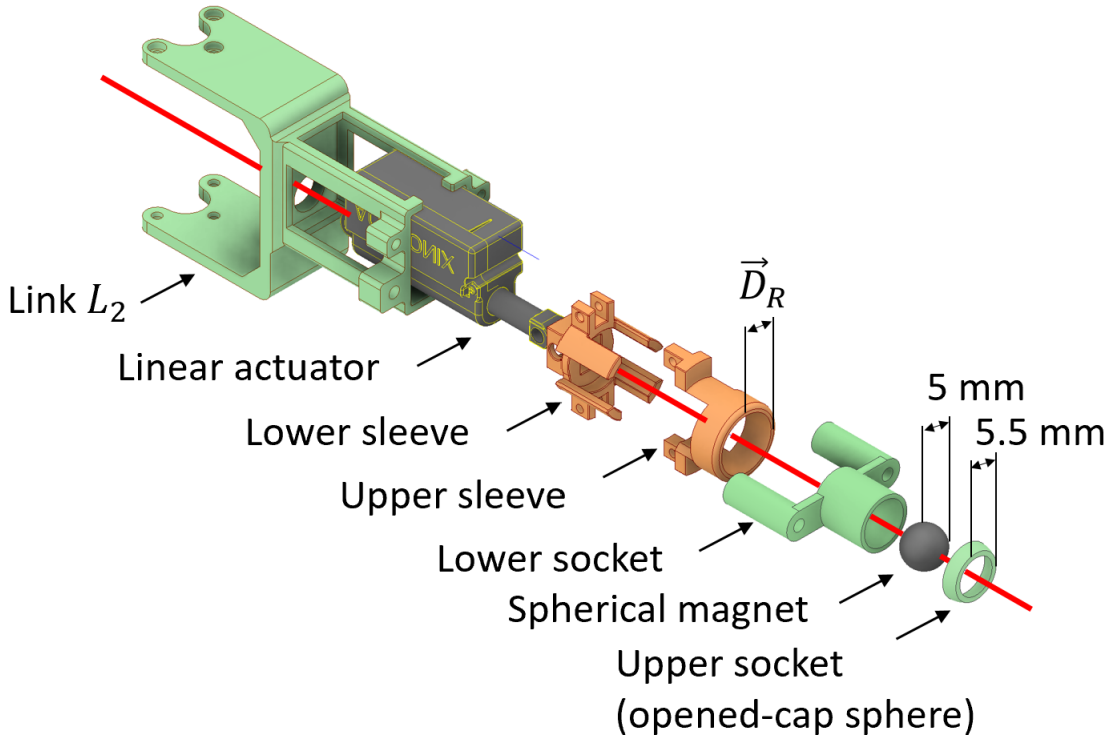

Figure 4.6. Component of the SMJ and adjustable sleeve.

4.3.5 Components of the robot's leg.

The legs of both robots have three DOF from three rotational servo actuators (Dynamixel XL430-W250-T) [33]. A spherical neodymium permanent (Nd-FeB) magnet with a radius of 5 millimeters [35] was implemented into the tip of each foot to create the attractive force $\vec{F}_M$ for the robot to hang in inverted locomotion.

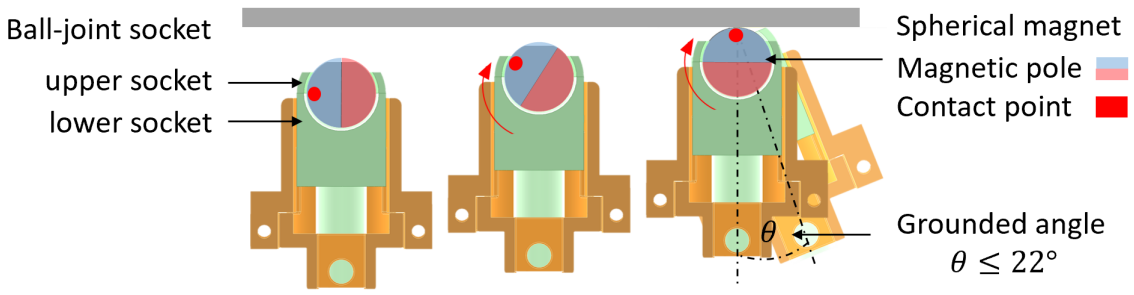

Figure 4.7. Activating of the attractive force and cross-section of the SMJ.

Table 4.2

Specification of the equipment

Equipment	Maximum load
Dynamixel XL430-W250-T	1.5 (N.m)
Actuonix PQ12-R	18 (N)
Permanent magnet (NdFeB)	7.4 (N)

As shown in Figure 4.6, the SMJ section shows how the SPM was placed inside the ball-joint socket which was created by an opened-cap 5.5 mm radius upper socket and assembling it with the lower socket using super glue. This allows the structure to tilt between $\theta \leq 22^{\circ}$ around the SPM while it maintains the same contact point with the maximum adhesive force at the flat surface.

Additionally, the adjustable sleeve mechanism *S* with a linear actuator (Actuonix PQ12-R) [36] has also been integrated to help the robot detach the tip of its feet from the steel surface during inverted locomotion. Each of the servo and linear actuator compositions is shown in Figure 2.3 and Table 4.2 shows the specifications of the robot legs.

4.4 Gait generation for inverted locomotion

Generally, legged robots are classified by the number of their legs. Each platform uses a unique gait and body structure to maneuver itself. For example, the two-leg climbing robot type [37] and [38] was mainly developed with inchworm locomotion, while, four legs robot [22] and [39] mostly imitate mammalian or reptilian gait to carry more payload and increase static stability. However, four-legged robots still have limited static stability during walking. Certain studies [40] and [28] have developed six-legged robots to solve the stability problem by increasing the number of legs and rearranging them to mimic insects, these robots aim to enlarge the support polygon. To validate the versatility of our proposed SMJ and adjustable sleeve, we have developed gait generation for inverted locomotion in both quadruped and hexapod robot gaits.

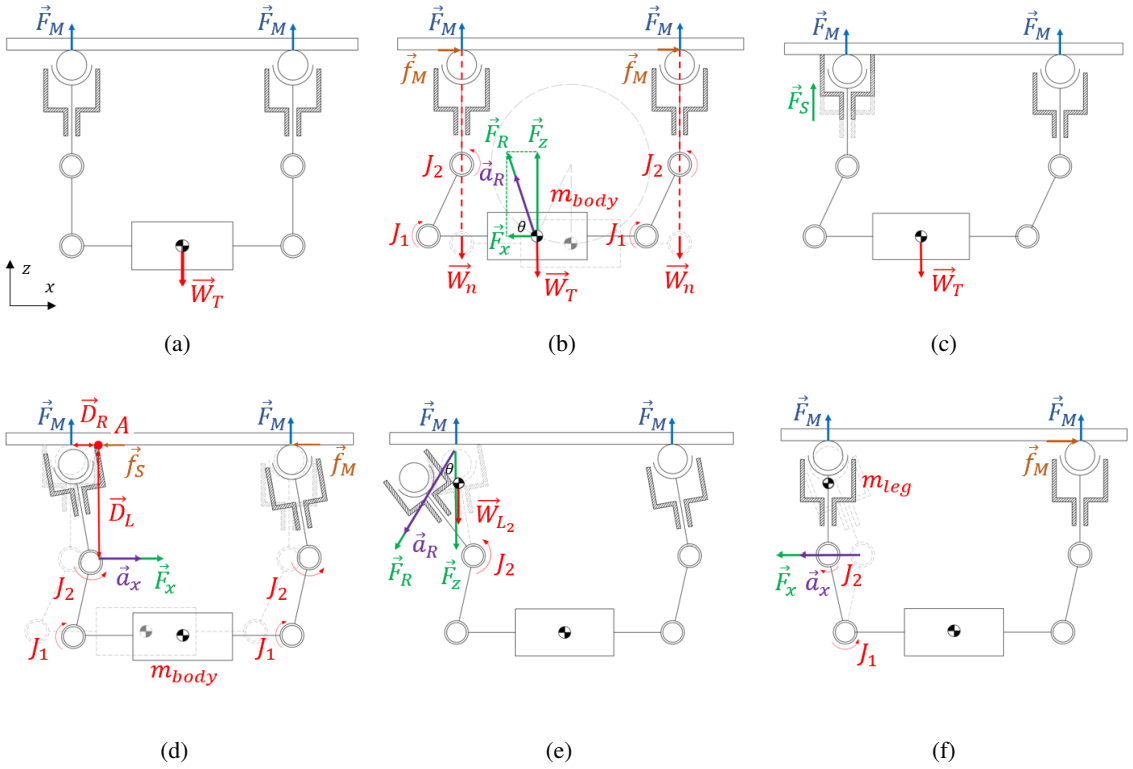

Figure 4.8. Postures of the robot. (a) Hanging posture. (b) Moving body. (c) Extending sleeve. (d) Tilting leg. (e) Detaching leg. (f) Placing leg.

In this section, the inverted gait generation will be described step by step, from each posture until the complete gait of each robot configuration. Starting from a hanging posture, a moving body, a detaching foot tip, and a placing foot tip. After that, The gait of each type of robot was constructed based on several detached legs in one detaching step to test the robot for inverted locomotion on a steel surface. There are two gaits for each robot configuration, a crawling gait and a trotting gait for a quadruped robot, and a square gait and a tripod gait for a hexapod robot.

4.4.1 Hanging posture

The first posture is a hanging, this can be constructed as a home posture of the robot. All of the legs were attached to the ceiling and a support polygon was created, with no actuated servo and external forces as shown in Figure 4.8(a).

We can assume from the FBD that $\sum \vec{F_M}$ reaches the highest value and the static stability was described as equation (4.5).

$$\sum_{n=1}^{N} \vec{F_M^n} \geqslant \vec{W_T} \tag{4.5}$$

4.4.2 Moving body

The second posture is a moving body, we design to move the robot body along the horizontal direction (x-axis) from the actuated joint servo as shown in Figure 4.8(b). From the FBD, a resultant force $\vec{F_R}$ can be calculated as in the equation (4.6).

$$\vec{F_R} = (m_{body})(\vec{a_R}) \tag{4.6}$$

where m_{body} is the mass of the robot body, $\vec{a_R}$ is a resultant acceleration from the actuator.

From the $\vec{F_R}$, the $\vec{F_x}$ and $\vec{F_z}$ can be calculated as in the equations (4.7) and (4.8).

$$\vec{F_x} = \vec{F_R} \cos\theta \tag{4.7}$$

$$\vec{F_z} = \vec{F_R} \sin\theta \tag{4.8}$$

In this state, we moved the body in the stable hanging pose with the support polygon. As a result, the robot will successfully move the body without falling or slipping as shown in equation (4.9).

$$\vec{f_M} \geqslant \vec{F_x} \tag{4.9}$$

where $\vec{f_M}$ is a static friction on the x-axis and can be varied depending on the equation (4.10)

$$\vec{f_M} = \mu_M(\vec{F_M} + \vec{F_z} - \vec{W_n}) \tag{4.10}$$

where μ_M is the friction coefficient between the SPM and the surface and $\vec{W}_n$ is the weight acting on each leg.

4.4.3 Detaching foot tip

The third posture is a detaching foot tip, this posture was developed based on lever tilting and pulling using an adjustable sleeve, as shown in Figure 3.7. This mechanism helps the robot pull its leg with less attractive force when the horizontal force $\vec{F}_x$ is applied through the leg while the robot crouches its body after the sleeve is extended.

From Figure 4.8, the robot must be in the hanging posture before detaching the leg due to the static stability of the posture. After that, the selected leg sleeve is stretched to the surface to create a fulcrum point A, as shown in Figure 4.8(c). Then the J_1 and J_2 actuators are rotated in opposite directions to apply the tangent force $\vec{F}_x$ from the circular motion of the link (L_2), using the tip of the foot as the center of rotation, as shown in Figure 4.8(d).

To successfully tilted the leg, the two required conditions must be met as described in section 2.2. Then the tip of the foot begins to tilt, as in the equation (4.11),

$$\vec{F}_x > \frac{\vec{D}_R}{\vec{D}_L} \times \vec{F}_M \tag{4.11}$$

where $\vec{F}_x$ can be adjusted by changing the acceleration of the actuator J_1 and J_2, as referred to in equation (4.12).

$$\vec{F}_x = (m_{body})(\vec{a}_x) \tag{4.12}$$

where m_{body} is the mass of the crouching body and $\vec{a}_x$ is an acceleration in the x-axis that can be adjusted from the actuator J_1 and J_2.

After the leg is tilted, the attractive force $\vec{F}_M$ decreases respectively, because the gap distance d between magnet and surface increases, as referred to in equation (3.2).

Finally, the actuator J_2 can detach the leg, as shown in Figure 4.8(e) by applying the $\vec{F}_R$ along with the help of the $\vec{W}_{L_2}$ weight of the link without generating a strong direct pulling force $\vec{F}_z$ during the detaching step referred to in the equation (4.13)

$$\vec{F}_R \cos\theta + \vec{W}_{L_2} > \vec{F}_M \tag{4.13}$$

where $\vec{F}_R$ is a resultant force from rotating link L_2 and $\vec{W}_{L_2}$ is a weight of the link L_2.

4.4.4 Placing foot tip

The fourth posture is a placing foot tip, after the leg was lifted, the robot swings the leg to form the support polygon at a new position. Normally, if the attached leg is forming the support polygon, the leg placing step will be stable as shown in Figure 4.8(f) and the equation (4.14).

$$\sum_{n=1}^{N} \vec{F}_x^n = (m_{leg})(\vec{a}_x) \tag{4.14}$$

where m_{leg} is the mass of the moving leg and $\vec{a}_x$ is an acceleration in the x-axis that can be adjusted from the actuator. However, in the case of two attached legs, the robot is stable only in two axes except the center line referred to the section 2.3.2. For this reason, the robot has a chance to be tilted perpendicular to the center line if the external force was applied as shown in Figure 4.1(b).

Combining the SMJ, the adjustable sleeve mechanism, and six robot postures, our robot platform fulfills the essentials for gait generation, as described in the next following section.

4.4.5 Quadruped robot gait

Duty factor

The quadruped robotic platform in this research is represents the minimum requirement of static stability during inverted the locomotion of a multi-legged robot.

Table 4.3

Duty factor of the quadruped robot

Duty factor	Number of the attached leg	Gait type
100%	4	-
75%	3	Static
50%	2	Dynamic

The criteria for the stability of the quadruped robot platform is called "Duty Factor (DF)" . This value represents the ratio of the attached leg L_a and the total leg L_t numbers, as shown in the (4.15) equation:

$$DF = \frac{L_a}{L_t} \tag{4.15}$$

The duty factor of the quadruped robot is shown in Table 4.3. The maximum number of the duty factor is 100%. If $DF \geqslant 75\%$, the robot gait is classified as a static gait, while $DF \geqslant 50\%$ is considered a dynamic gait. Therefore, the number of detached legs during locomotion will define the stability of the robot.

Referred to the stability section 4.2, The attached leg of the quadruped robot during the inverted locomotion are the same as the double legs and triple legs or more conditions as shown in Figure 4.1(b) and Figure 4.1(c). Thus, the body of the robot can be tilted while hanging with two legs. However, it will be stable if the leg is attached with triple legs or more.

Moreover, the support polygon or support line is created by the number of the attached legs during the detached, step as shown in Figure 4.9. This support polygon area or support line determines the stability of the robot depending on the position of the Center of Mass (COM) in the support area. Hence, the robot remains stable if the COM position is inside the support area or support line. However, it will be unstable if the COM is outside of the support area or support line. For these reasons, the crawling gait is considered to be the static gait, and the trotting gait is considered to be the dynamic gait for the quadruped robot.

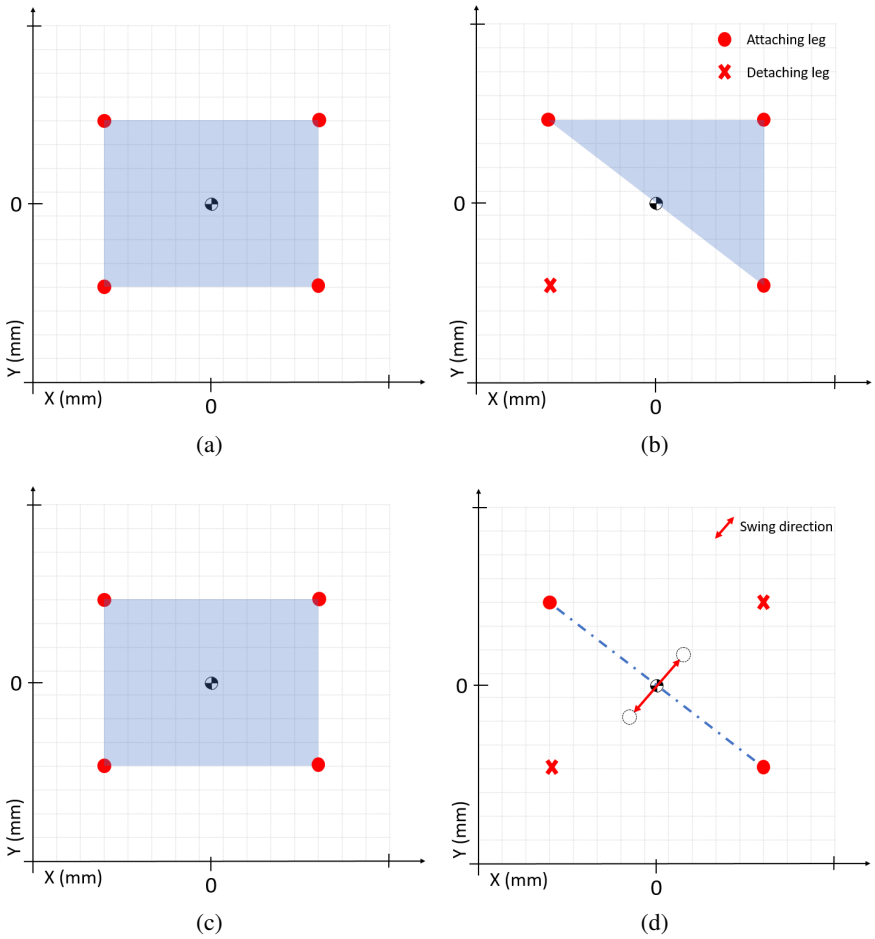

Figure 4.9. (a) Support polygon of the quadruped robot crawling gait. (b) Support polygon of the trotting gait. (c) Support polygon of the detaching step. (d) Support line of the trotting gait.

Crawling gait

The crawling gait was designed for the inverted locomotion of the quadruped robot. This gait is categorized as a static gait because the duty factor $DF \geqslant 75\%$ is calculated based on the three attached legs L_a while the detached leg moves. The COM of the robot is not required to stay inside the triangle support polygon due to the attractive force $\vec{F_M}$, as shown in Figure 4.10. This helps the robot to stabilize itself while moving.

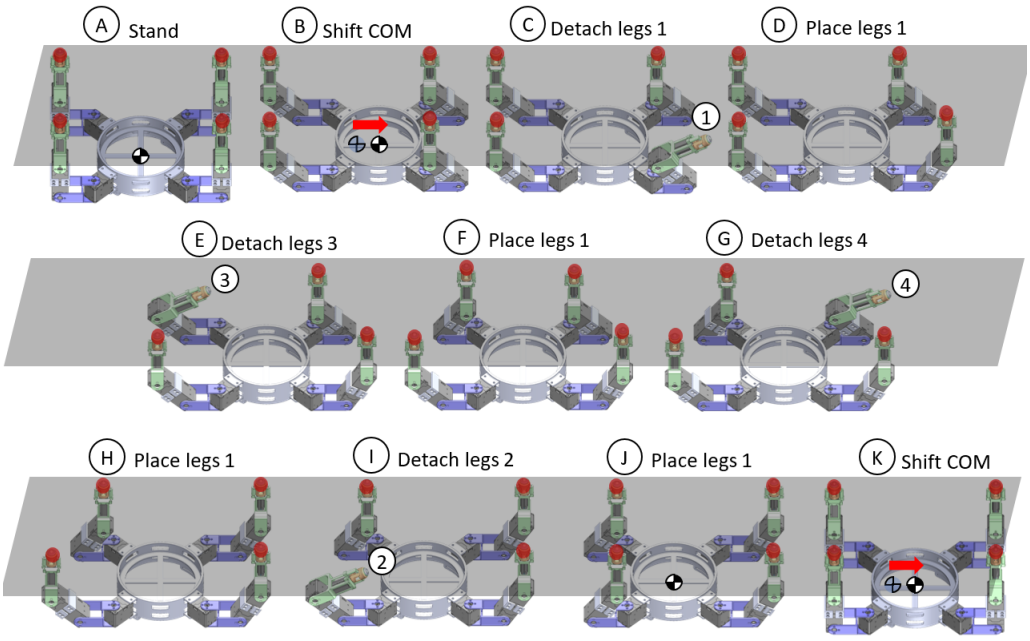

Figure 4.10. Crawling gait. This figure shows the detached leg, the attached leg, and the robot's COM for each step of the crawling gait.

The first sequence starts with the mammal-type stance for the home position (The hanging pose), as shown in step (A) of Figure 4.10. Then, the body will shift toward the desired direction (Moving the body), as shown in the next step (B). After that, the robot pulls leg 1 by the detached step (C) and constructs a new point of the triangle support polygon in step (D) (Placing foot tip). From step (E) to (J), the detached foot performs on the other legs until they are moved to a new location. Finally, the robot shifts the body to the first step (K) to restart the new gait cycle.

Trotting gait

In this gait, the robot performs a dynamic gait by detaching two legs simultaneously during the detaching step. This gives a duty factor of $DF \geqslant 50\%$. The moving of the body and the hanging posture of the robot are the same as the crawling gait, except the number of detached legs changes the support polygon to a support line, as shown in Figure 4.11. Therefore, this reduces the number of steps to complete the cycle of the robot's gait. The trotting gait of the robot is described in Figure 4.11. First, the robot stands in the home position and moves

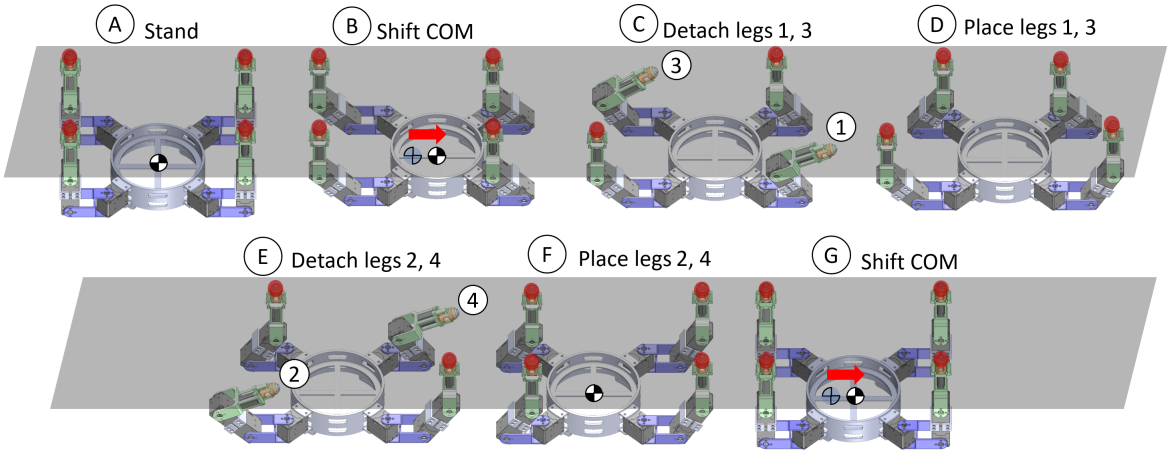

Figure 4.11. Trotting gait. This figure shows the detached leg, the attached leg, and the robot's COM for each step of the trotting gait.

its body toward the goal direction, as shown in steps (A) and (B). Then, the leg pair 1 and 3 detach in step (C). After that, the detached pair of legs, 1 and 3, are placed in the new position in step (D). The detaching step is performed again by the other pair of legs in steps (E) and (F). Finally, the robot shifts the body in step (G) and resets the cycle. During locomotion, the robot might swing in the perpendicular direction of the support line as referred to as the stability of the double legs configuration.

4.4.6 Hexapod robot gait

The hexapod platform was selected, as the maximum number of legs always guarantees the stability of the robot while performing the detaching step. Adding two more legs to the quadruped robot can preserve the robot's COM to remain inside the support polygon in every constructed gait, as shown in Figure 4.12. Hence, there is no need to calculate a duty factor for this robot type. We validate two hexapod gaits "square gait and tripod gait" for the inverted locomotion. The differences between the two gaits are the number of detached legs while performing the detaching step and the shape of the support polygon.

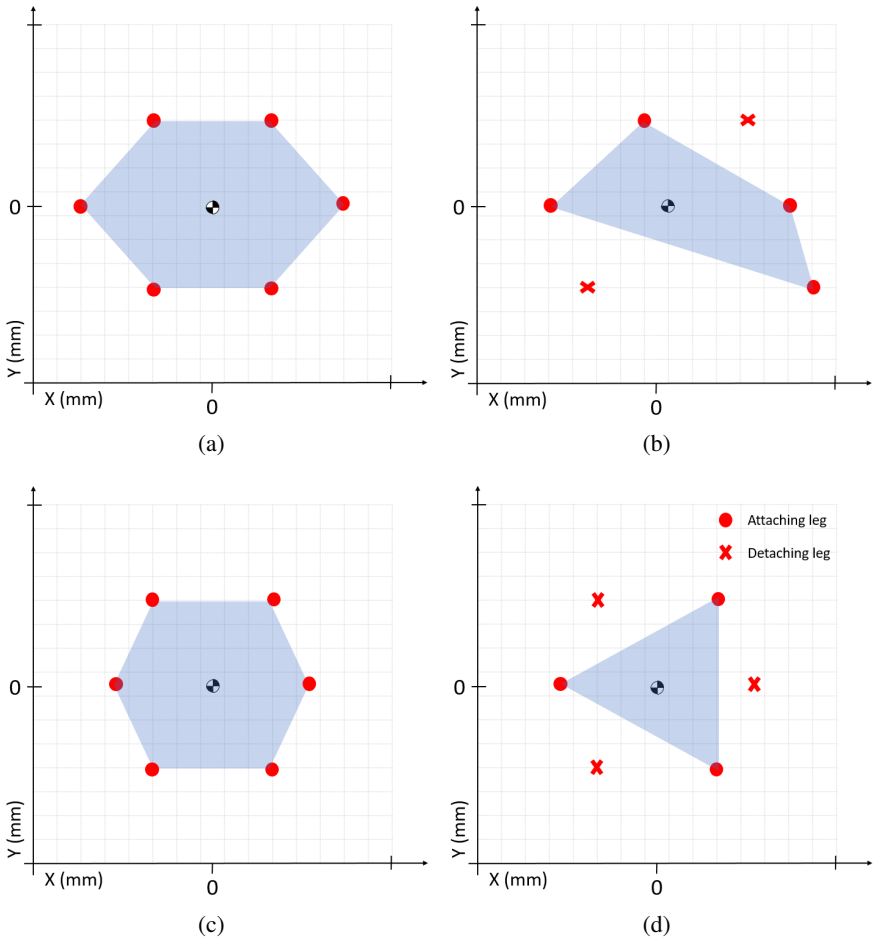

Figure 4.12. (a) Support polygon of the hexapod robot square gait. (b) Support polygon of the square gait detaching step. (c) Support polygon of the hexapod robot tripod gait. (d) Support polygon of the tripod gait detaching step.

Square gait

For the square support gait, the home position of the robot is the hexagonal shape with a greater length, as shown in Figure 4.13. The movement process starts with the moving of the robot's body toward the goal direction followed by moving a pair of legs to complete the cycle.

First, the robot starts from the home position, as shown in step (A). Then the robot's body shifts to the locomotion direction, as shown in step (B). After that, the detaching step is performed with legs 3 and 6, which swing to a new position in steps (C) and (D).

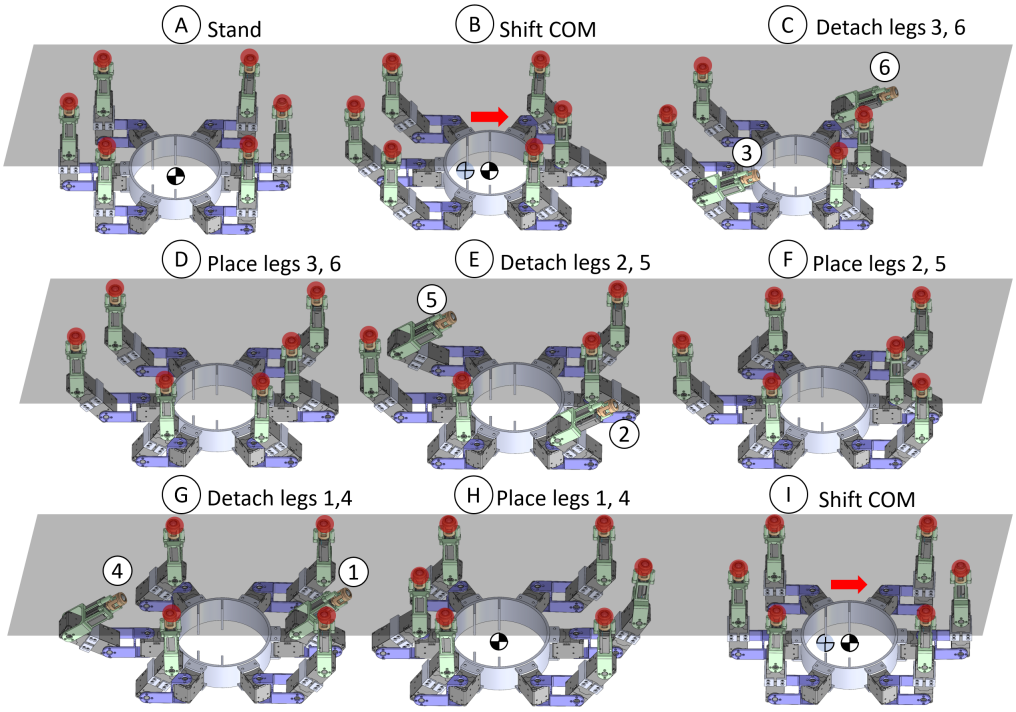

Figure 4.13. Square gait. This figure shows the detached leg, the attached leg, and the robot's COM for each step of the square gait.

The leg swing step repeats and changes to the other legs in steps (E) to (H). Finally, the robot shifts its body to a new home position in step (I) to restart the cycle until reaching the goal.

Tripod gait

In this gait, the robot's home position is different from the previous gait. The home position is a symmetrical hexagon, as shown in Figure 4.14. Hence, the gait cycle can start by detaching three legs in one step before moving the body.

The first step (A) of the robot is the home position. Then, legs 1,3, and 5 are pulled from the surface by performing the detaching step (B). After that, the body of the robot shifts toward the goal direction by moving legs 2,4, and 6 in step (C). The detaching step repeats with legs 2,4, and 6 in step (D) and swings to the new home position to restart the robot's gait cycle in steps (E) and (F).

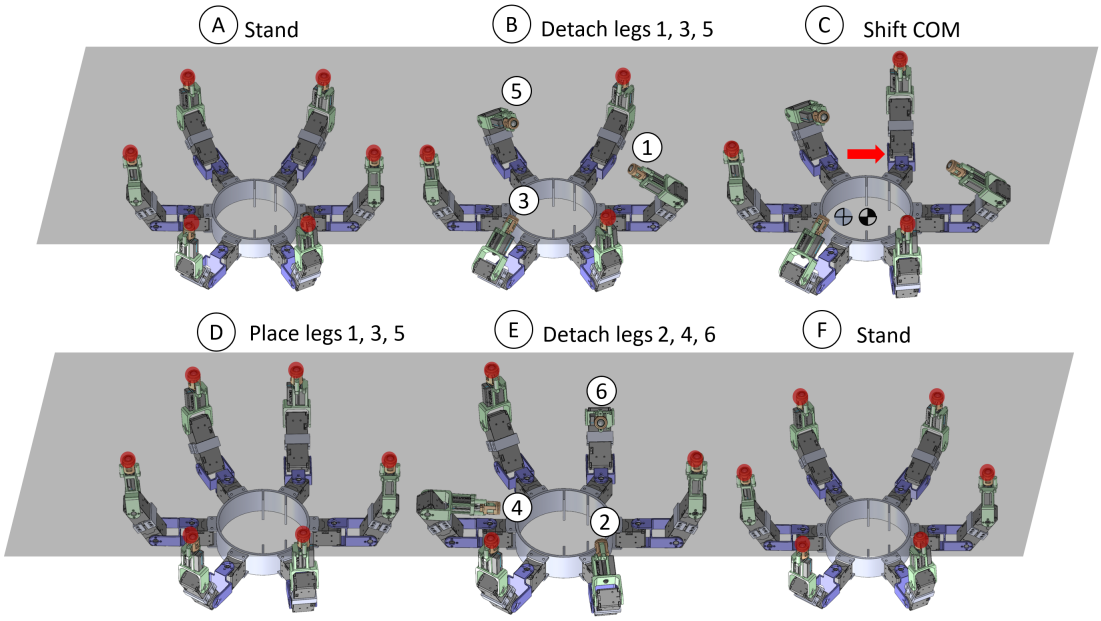

Figure 4.14. Tripod gait. This figure shows the detached leg, the attached leg, and the robot's COM for each step of the tripod gait.

Table 4.4

Friction and Coefficient of friction.

Posture	Coefficient	Friction(N)
Moving the body	$\mu_M = 0.28$	1.6
Detaching leg	$\mu_S = 0.46$	3.4

After generating all the gaits for each of the configurations, the following section describes the experiment that was conducted to compare and verify the robot's stability, velocity, and accuracy in each different gait generation.

4.5 Experiment: Inverted locomotion

To guarantee that the robot's foot will not slip during locomotion, we calculate the static friction between the contact surfaces, such as $\vec{f_S}$ and $\vec{f_M}$. The coefficients of friction, μ_M and μ_S were measured to determine the maximum applied force for the conditions described in section 3.4 (tilting the foot) and section 4.4.2 (moving the body), as shown in the Table 4.4

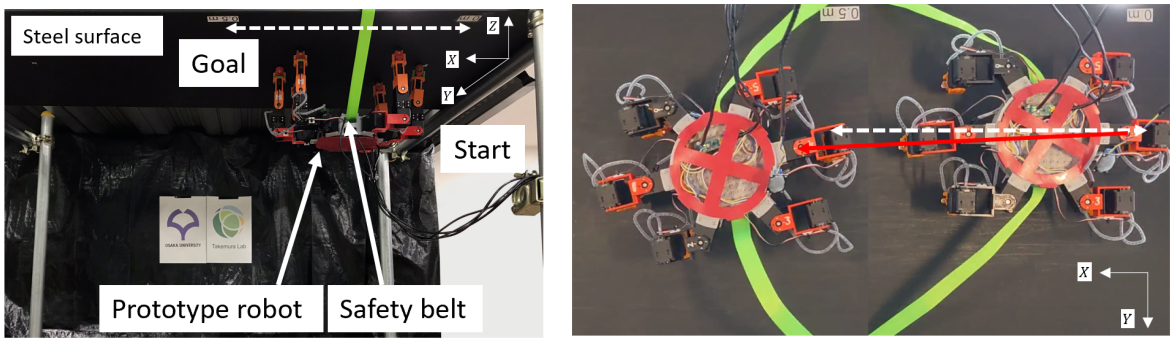

(a) (b)

Figure 4.15. Experiment setup of the inverted locomotion: (a) Equipment and robot setup. (b) Bottom view for a path and COM tracking.

The inverted locomotion of the robot was conducted using a setup under a steel surface, as shown in Figure 4.15. The distance between the starting point and the goal point was 50 centimeters. The experiment was separated into four sub-experiments: the crawling gait, the trotting gait, the square gait, and the tripod gait. The robots walked 10 times for each gait, and the locomotion path was collected through bottom and side view cameras.

Crawling gait

The crawling gait experiment was implemented using the quadruped robot, and a complete cycle of the gait was separated into 11 steps, as shown in Figure 4.16. In one cycle, the robot shifted the COM two times (steps (B) and (K)). Each of the steps shifted 5 cm, as shown in Figure 4.20(a). Therefore, the velocity of this robot is 0.23 cm/s, shown in Figure 4.21. The path of the robot was plotted in Figure 4.22(a).

As seen from the robot's path, this gait showed the maximum drifted distance (8.20 cm) from the reference line on the y-axis with an error range of 1.60 cm due to the leg slipping and turning moments during the leg detaching step. Especially at step (G), the support polygon is in the shape of a scalene trapezoid. When detaching the 4^{th} leg, a significant turning moment occur in a *CCW* direction, which causes the robot to rotate to the shorter side of the scalene trapezoid, as shown in Figure 4.23(a).

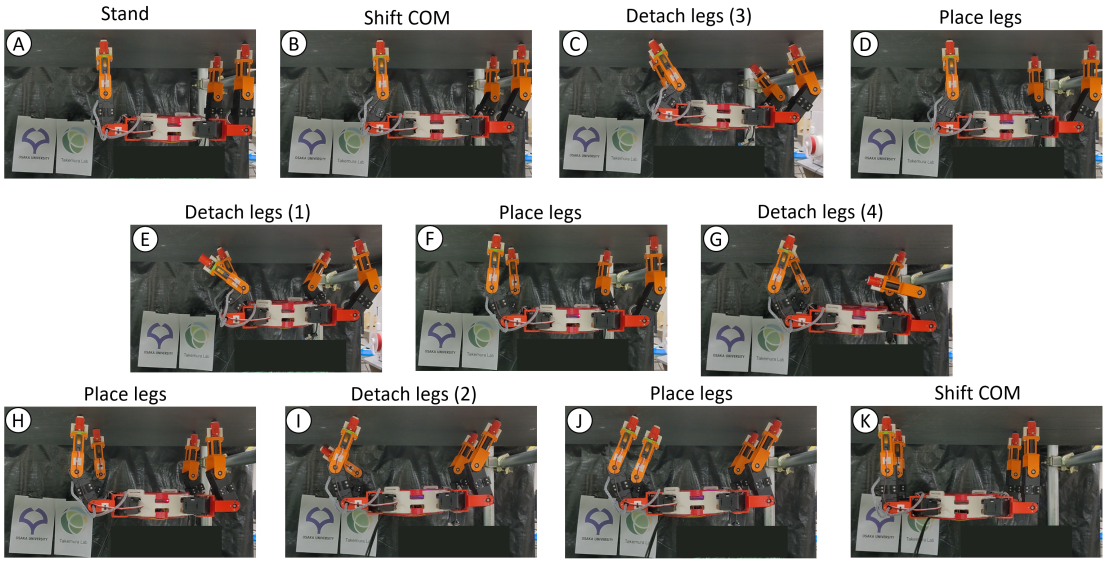

Figure 4.16. Crawling gait. This figure shows the crawling gait of the robot during the experiment for inverted locomotion.

Trotting gait

The other gait to test the inverted locomotion of the quadruped robot is the trotting gait. The walking robot was captured step by step, as shown in Figure 4.17. The differences between the crawling gait and the trotting gait are the support structure and the number of pulling legs in detaching steps (C) and (E), as shown in Figure 4.10 and Figure 4.11. Due to fewer steps, the velocity of the robot reached 0.64 cm/s, as shown in Figure 4.21, and the path of this robot was plotted in Figure 4.22(b).

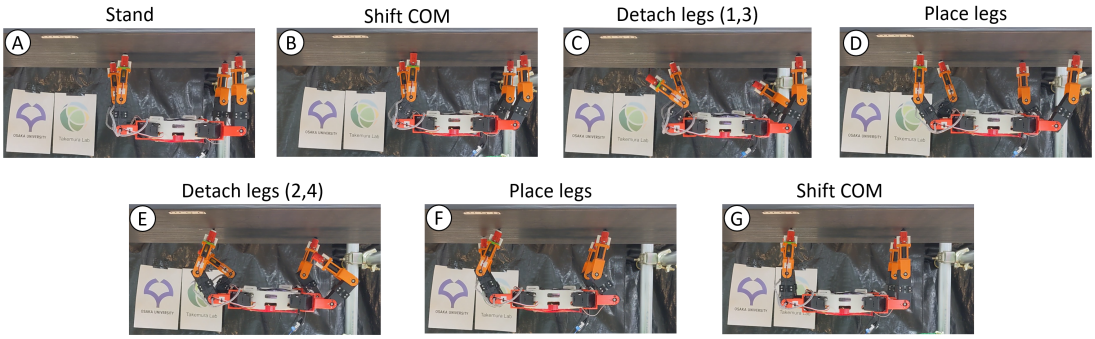

Figure 4.17. Trotting gait. This figure shows the trotting gait of the robot during the experiment for inverted locomotion.

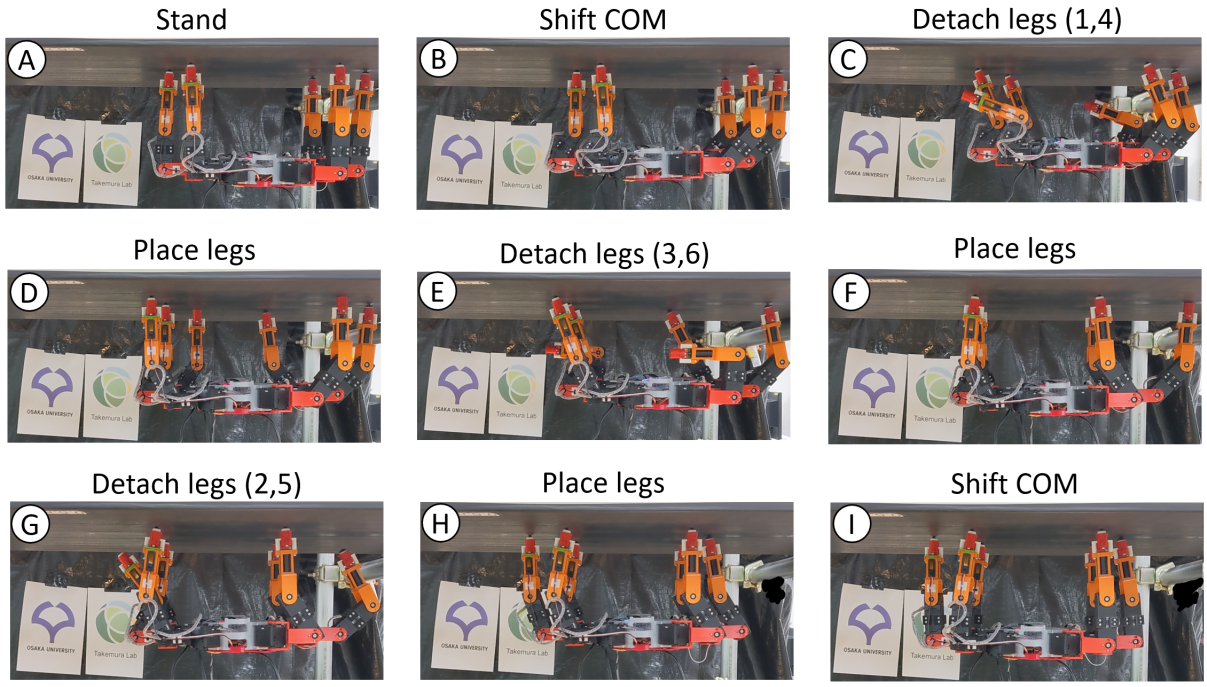

Figure 4.18. Square gait. This figure shows the square gait of the robot during the experiment for inverted locomotion.

As seen from the robot's path, this gait had the minimum drifted distance (2.10 cm) among the four gaits, with an error range of 0.21 cm. Though the direction of the drift was the same as that of the crawling gait, this gait drifted a smaller distance, and there was an error because the turning moment of the robot's body was very small due to the two detached leg pairs (1,3 and 2,4), which were always counterbalanced as shown in Figure 4.23(b).

Square gait

In contrast to the rest of the experiments, this robot platform was changed to a hexapod platform by adding two more legs around the robot's body. The experiment of the hexapod robot started with the square gait, and each of the steps was captured, as shown in Figure 4.18. The detaching step of this gait pulls a pair of legs in one detaching, steps (C), (F), and (G). The remaining legs still attach to the surface and form a square-shaped support polygon, as shown in Figure 4.13.

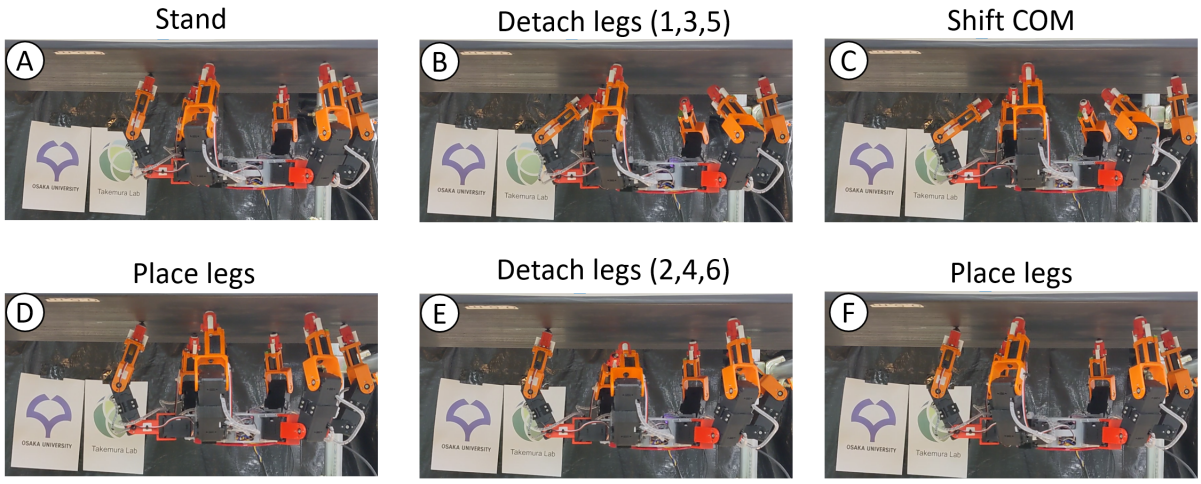

Figure 4.19. Tripod gait. This figure shows the tripod gait of the robot during the experiment for inverted locomotion.

The robot shifted the COM 4 cm in one shift, steps (B) and (I). Even though the leg arrangement and the shape of the robot are different from the quadruped robot, the shifting methods were similar to each other, as shown in Figure 4.20(c). Therefore, the velocity of this robot was 0.32 cm/s, as shown in Figure 4.21, and the path of this robot was plotted in Figure 4.22(c).

As seen from the robot's path, this gait had a drifted distance on the y-axis of 6.10 cm, with an error range of 1.14 cm. Especially at step (E), the support polygon was irregular and had an asymmetrical hexagonal shape. When detaching the 3^{th} and the 6^{th} legs, a significant turning moment occur in a *CCW* direction which caused the robot to rotate toward the *CCW* direction, as shown in Figure 4.23(c). However, the middle pair of the hexapod robot legs formed a more stable support polygon than the quadruped robot. As a result, the drifted distance and the error in the robot's path were smaller than the crawling gait of the quadruped robot.

Tripod gait

Finally, the hexapod robot's inverted locomotion was performed using the tripod gait. Each of the steps was captured, as shown in Figure 4.19.

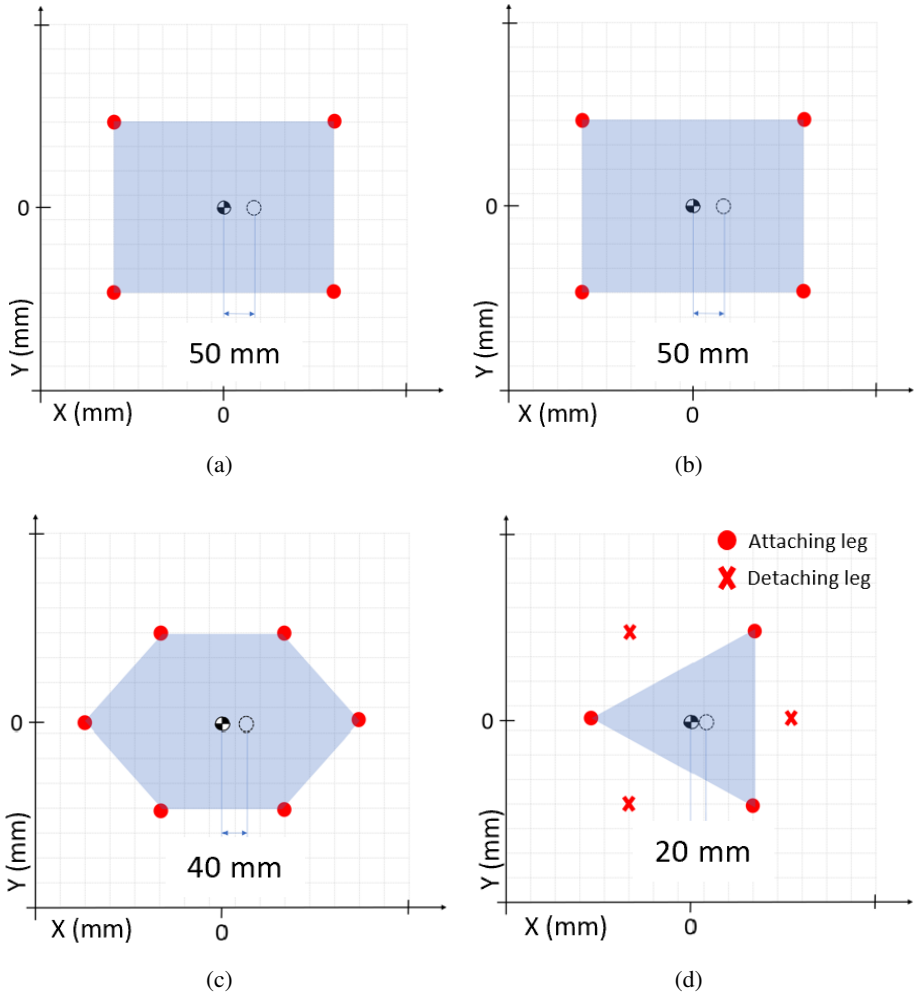

Figure 4.20. COM tracking of the inverted locomotion experiment: (a) Crawling gait of the quadruped robot. (b) Trotting gait of the quadruped robot. (c) Square gait of the hexapod robot. (d) Tripod gait of the hexapod robot.

This gait was performed using three detaching legs in one detaching step (B) and (E) to prove the maximum pulling legs of the hexapod robot. The supported triangle during the detaching step is plotted in Figure 4.14, and the COM shifting step (C) is also plotted in Figure 4.20(d). However, the COM moved a small distance of 2 cm due to the leg arrangement and smaller attractive force $\vec{F_M}$. As a result, the velocity of the robot was reduced to 0.18 cm/s, as shown in Figure 4.21, and the path of this robot was plotted in Figure 4.22(d).

As seen from the robot's path, this gait has a drifted distance on the y-axis of 3.40 cm, with an error range of 0.43 cm.

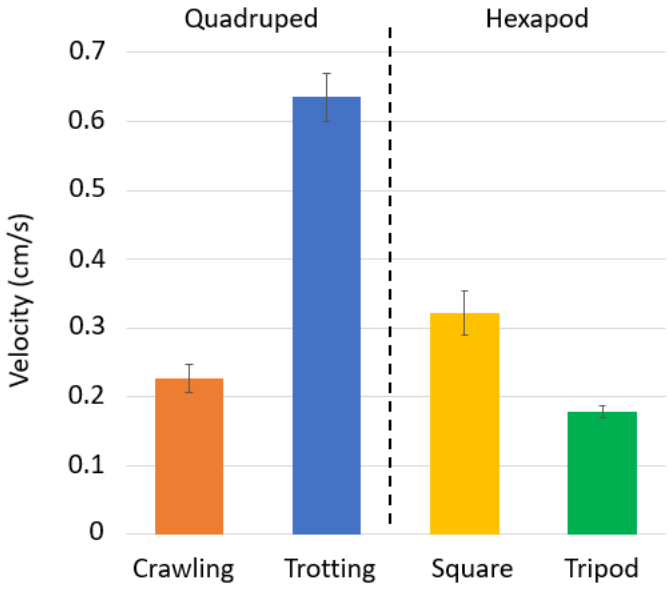

Figure 4.21. Robot velocity. This figure shows the robot's average velocity during each gait from the inverted locomotion 50 cm goal.

The detaching step of this gait was different from all other gaits. Since the detaching legs were pulled toward the center of the robot of the symmetrical support polygon, as shown in Figure 4.23(d), the robot body did not rotate and kept moving forward on the x-axis. The majority of drifting from the reference line was only from the leg slipping during the COM shifting in step (C).

4.6 Discussion

In the inverted locomotion experiment, all of the robot platforms were successfully conducted under the steel surface. Each gait had different detaching and COM shifting steps. Though the hanging stability of the crawling gait was better than the trotting gait due to the formation of the support polygon and high total attractive force $\vec{F_M}$ from the attached leg as shown in Figure 4.23, the trotting gait showed better locomotion than the crawling gait in terms of velocity (0.64 cm/s) and path accuracy (SD = 0.21 cm).

For the hexapod robot, the hanging stability of the square gait was better than the tripod gait due to the total attractive force $\vec{F_M}$ from the attached leg during the detaching step in Figure 4.23.

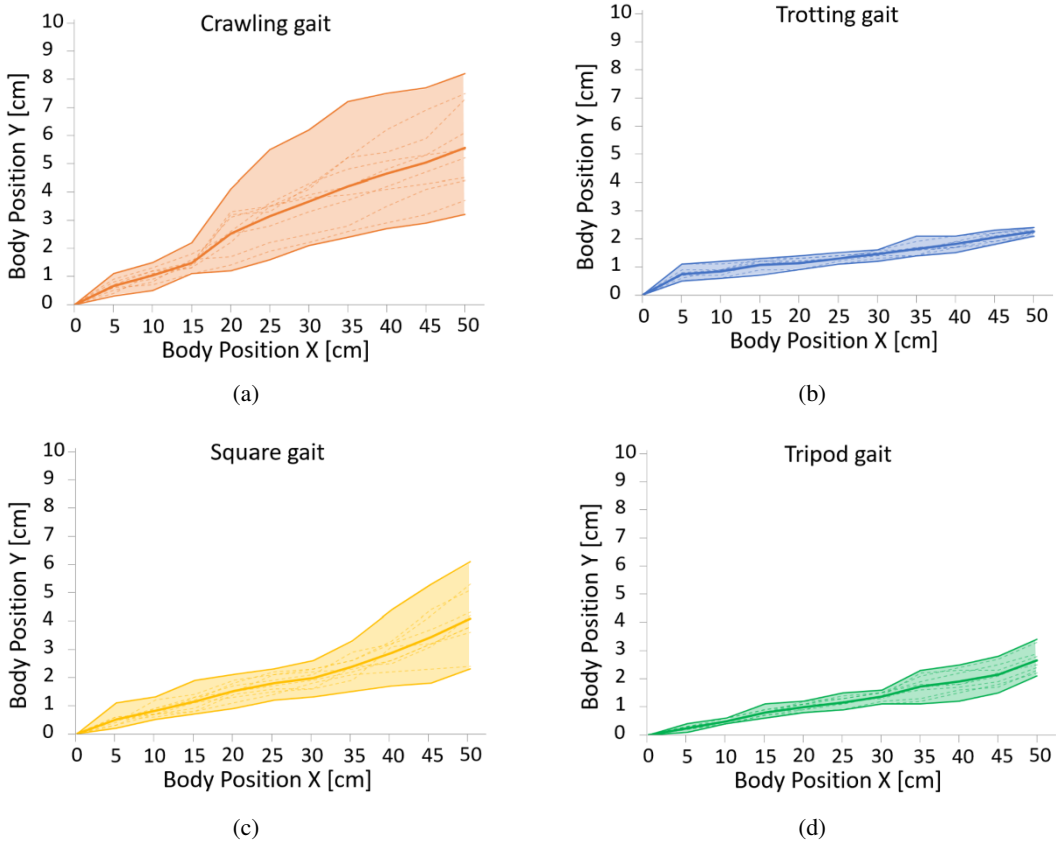

Figure 4.22. Robot trajectory of the inverted locomotion experiment: (a) Crawling gait of the quadruped robot. (b) Trotting gait of the quadruped robot. (c) Square gait of the hexapod robot. (d) Tripod gait of the hexapod robot.

Also, the accuracy of the tripod gait (SD = 0.43) was better than the square gait (SD = 1.14). However, during locomotion, the velocity of the square gait (velocity of 0.32 cm/s) was better than the tripod gait (velocity of 0.18 cm/s).

The unexpected drifting during locomotion was captured and plotted in Figure 4.22. The inaccuracy of foot placement between single steps can be accumulated and expanded in a long-run distance. These noticeable errors were created by two major concerns. First, without force control, the precise amount of real force from the actuator and attractive force $\vec{F_M}$ were not acquired during locomotion. Since the error from foot placement occurred when there was an immediate change from the weak to the strong attractive force, force control should be considered for precision control of leg placement.

The second concern was the friction between the surface and the tip of the foot when the robot placed or detached its leg. The coefficient of friction of the plastic material we used was not enough to create a static frictional force; therefore, the robot could slip and gradually drift off of the track. To solve this problem, a rigid material with the properties of a higher coefficient of friction and continuity of applying friction force at the fulcrum point to prevent the slippage of the robot should be used to create a robust sleeve.

4.7 Conclusion

The author also proposed four different gait generations for quadruped and hexapod robots based on the spherical magnetic joint and the adjustable sleeve.

From gait generation analysis, it was observed that the trotting gait achieved the highest velocity of 0.64 cm/s and drifted the smallest distance among the four gaits, 2.10 cm. In contrast, the crawling gait had more hanging stability but was slower (velocity of 0.23 cm/s) and drifted a larger distance of 8.20 cm. However, the square gait and tripod gait of the hexapod robot had higher hanging stability than the quadruped robot due to a larger number of legs. This platform would be suitable for a tasking that requires a high payload. However, the locomotion velocity was lower than the trotting gait, with velocities of 0.32 cm/s and 0.18 cm/s, respectively.

4.8 Contribution

The contributions of the work presented in this chapter were:

- Gait generation for inverted locomotion, the proposed gaits for each of the multi-legged robots were successfully performed the inverted locomotion along with the versatility for different tasking in terms of velocity, stability, and accuracy.

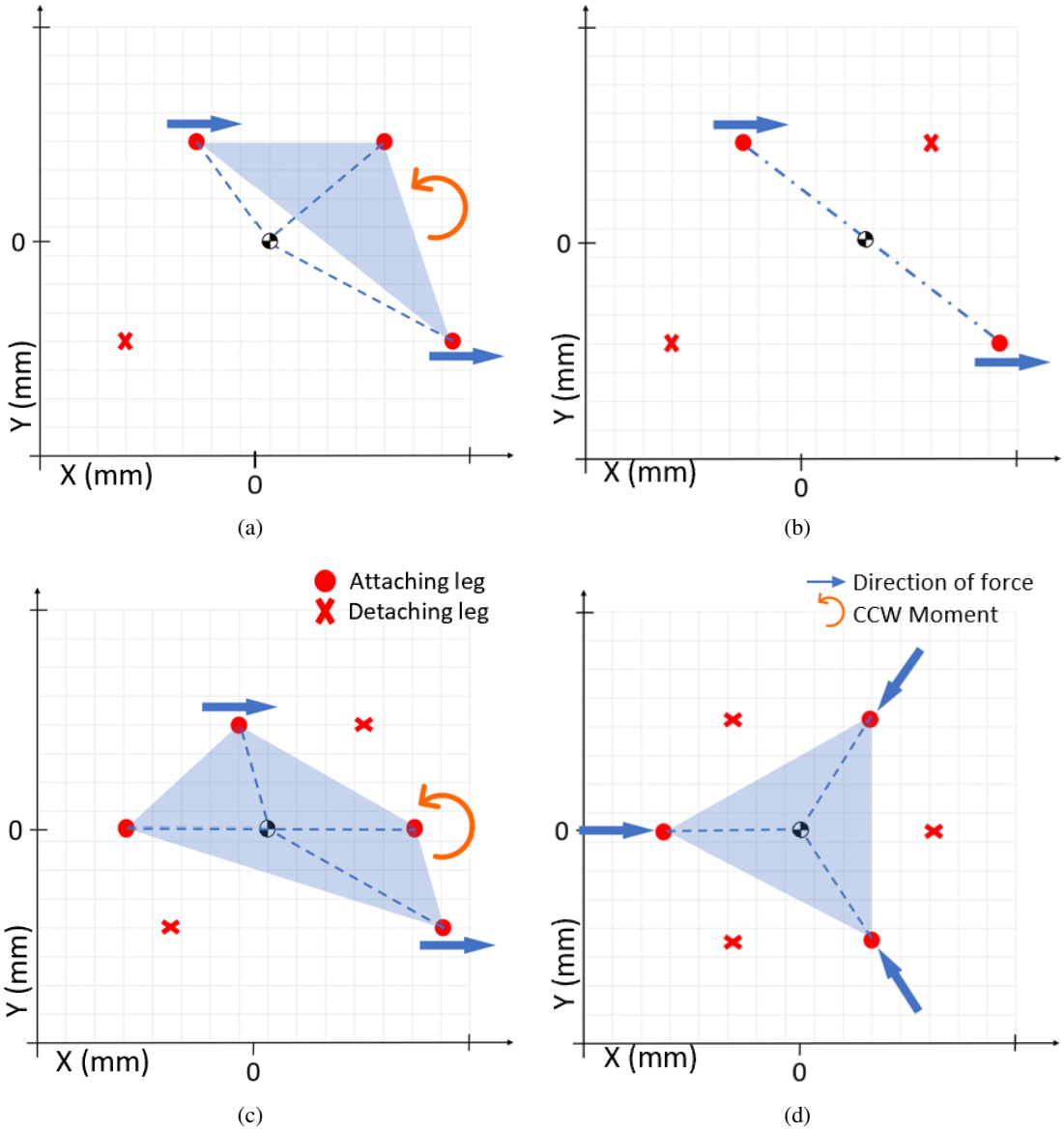

Figure 4.23. Applied forces and support polygon during detaching step: (a) Crawling gait of the quadruped robot. (b) Trotting gait of the quadruped robot. (c) Square gait of the hexapod robot. (d) Tripod gait of the hexapod robot.

Chapter 5

Conclusion

As described in Section 1.6, This chapter will conclude the study by addressing the major research findings concerning the research questions, philosophies, and contributions. The limitations of the study will be discussed along with suggested ideas for further research.

5.1 Summary of Major Findings

This study aimed to develop a Spherical Magnetic Joint (SMJ) based on the spherical permanent magnet that allows robust and flexible adhesive force on the steel surface. As a result, the inverted locomotion of a multi-legged robot for the steel structural inspection is achieved. The study begins with an analysis of the suitable type and shape of the permanent magnet. Afterward, the design of the adjustable sleeve with the important design parameters is determined based on an observation of the pulling force. Finally, four inverted locomotion gaits were constructed for two different robot platforms, and evaluate each of the gaits by comparing the movement velocity, stability, and accuracy.

In Chapter 3, the results of the spherical magnetic joint showed that the characteristic of the spherical permanent magnet provides the maximum attractive force with the small tangent area between the magnet and the surface. The comparison between the ball joint and fixed joint connection proves that the flexibility of the ball joint allows the spherical permanent magnet to maintain the maximum attractive force while the fixed joint reduce the attractive force related to the angle.

Furthermore, the tilting and pulling present load result indicates that the load was decreased due to the tilting with the sleeve radius distance parameter $\vec{D_R}$. Hence, the spherical magnetic joint and the adjustable sleeve were presented in this work as one of the contributions of the robust and flexible adhesive device for the steel structural inspection multi-legged robot.

In Chapter 4, the evaluation of four gaits based on the spherical magnetic joint of the quadruped robot and hexapod robot showed that the trotting gait of the quadruped robot shifted with the smallest distance of 2.10 cm and reached the highest velocity of 0.64 cm/s of the four gaits. In contrast, the crawling gait of the hexapod robot had more stability due to having the three support legs for the support polygon but was slower and drifted a larger distance. Moreover, the square gait and tripod gait of the hexapod robot had higher static and dynamic stability from a larger number of legs. This configuration of the multi-legged robot would be suitable for a tasking that requires a large payload. Unlike the quadruped robot, the gait velocity was lower than the trotting gait, with velocities of 0.32 cm/s and 0.18 cm/s respectively. Therefore, the design and development of the gait for the inverted locomotion have versatility for handle difference working conditions depending on the user's requirement.

Referring to the research question and philosophy, the author wants to develop a steel structural inspection multi-legged robot that has the flexibility to maintain the attraction force while performing different postures and is able to lift the robot's foot without applying high torque. The SMJ and adjustable sleeve in Chapter 3 consist of the flexibility and controllability philosophies to answer those questions. Furthermore, the crawling gait, trotting gait, square gait, and tripod gait of the quadruped and hexapod robot were successfully delivered to the multi-legged robot from the start point to the goal point with the stability and versatility to be adapted in different scenarios.

During the experiment, an unexpected drift from inverted locomotion was observed. This is due to the open loop control and the non-ideal friction. These were considered a limitation of the permanent magnet. Since the attractive force control of the permanent magnet cannot be controlled directly, the proposed indirect method will generate a small error from the control mechanism.

Also, the coating material of a permanent magnet is expected to be cracked during foot placement. This will lead to an unexpected change in friction as well.

5.2 Future Study

The system is expected to be improved with feedback from sensors, such as force sensors and distance sensors to collect and analyze force and distance feedback data in order to design a suitable closed-loop control for the inverted locomotion of the robot. Moreover, the mechanism or the shape of the adjustable sleeve can be improved to be able to adjust the sleeve radius distance $\vec{D_R}$ and reduce the load of the driven actuator increasing the robot's stability during the detaching step. Similarly, several adjustable sleeve materials can also be tested and verified to prevent leg slip during inverted locomotion.

Bibliography

[1] R. S. Lim, H. M. La, Z. Shan, and W. Sheng, "Developing a crack inspection robot for bridge maintenance," in *2011 IEEE International Conference on Robotics and Automation*, pp. 6288–6293, IEEE, 2011.

[2] A. Leibbrandt, G. Caprari, U. Angst, R. Y. Siegwart, R. J. Flatt, and B. Elsener, "Climbing robot for corrosion monitoring of reinforced concrete structures," in *2012 2nd International Conference on Applied Robotics for the Power Industry (CARPI)*, pp. 10–15, IEEE, 2012.

[3] P. Quin, G. Paul, and D. Liu, "Experimental evaluation of nearest neighbor exploration approach in field environments," *IEEE Transactions on Automation Science and Engineering*, vol. 14, no. 2, pp. 869–880, 2017.

[4] G. Klancar, A. Zdesar, S. Blazic, and I. Skrjanc, *Wheeled mobile robotics: from fundamentals towards autonomous systems*. Butterworth-Heinemann, 2017.

[5] W. Fischer, G. Caprari, R. Siegwart, and R. Moser, "Compact magnetic wheeled robot for inspecting complex shaped structures in generator housings and similar environments," in *2009 IEEE/RSJ International Conference on Intelligent Robots and Systems*, pp. 4116–4121, IEEE, 2009.

[6] F. Tâche, F. Pomerleau, W. Fischer, G. Caprari, F. Mondada, R. Moser, and R. Siegwart, "Magnebike: Compact magnetic wheeled robot for power plant inspection," in *2010 1st International Conference on Applied Robotics for the Power Industry*, pp. 1–2, IEEE, 2010.

[7] M. Eich, F. Bonnin-Pascual, E. Garcia-Fidalgo, A. Ortiz, G. Bruzzone, Y. Koveos, and F. Kirchner, "A robot application for marine vessel inspection," *Journal of Field Robotics*, vol. 31, no. 2, pp. 319–341, 2014.

[8] A. Kakogawa and S. Ma, "Design of an underactuated parallelogram crawler module for an in-pipe robot," in *2013 IEEE International Conference on Robotics and Biomimetics (ROBIO)*, pp. 1324–1329, IEEE, 2013.

[9] E. Magid, T. Tsubouchi, E. Koyanagi, and T. Yoshida, "Static balance for rescue robot navigation: Losing balance on purpose within random step environment," in *2010 IEEE/RSJ International Conference on Intelligent Robots and Systems*, pp. 349–356, IEEE, 2010.

[10] J. Ramos and S. Kim, "Dynamic bilateral teleoperation of the cart-pole: a study toward the synchronization of human operator and legged robot," *IEEE Robotics and Automation Letters*, vol. 3, no. 4, pp. 3293–3299, 2018.

[11] Y. Liu, D. Lee, H. Kim, and T. Seo, "Compliant wall-climbing robotic platform for various curvatures," in *2015 IEEE/RSJ International Conference on Intelligent Robots and Systems (IROS)*, pp. 532–537, IEEE, 2015.

[12] J. Whitman, S. Su, S. Coros, A. Ansari, and H. Choset, "Generating gaits for simultaneous locomotion and manipulation," in *2017 IEEE/RSJ International Conference on Intelligent Robots and Systems (IROS)*, pp. 2723–2729, IEEE, 2017.

[13] A. Boonyaprapasorn, T. Maneewarn, and K. Thung-Od, "A prototype of inspection robot for water wall tubes in boiler," in *Proceedings of the 2014 3rd International Conference on Applied Robotics for the Power Industry*, pp. 1–6, IEEE, 2014.

[14] T. Arai, K. Kamiyama, P. Kriengkomol, Y. Mae, M. Kojima, and M. Horade, "Inspection robot in complicated 3d environments," in *ISARC. Proceedings of the International Symposium on Automation and Robotics in Construction*, vol. 32, p. 1, IAARC Publications, 2015.

[15] P. Ward and D. Liu, "Design of a high capacity electro permanent magnetic adhesion for climbing robots," in *2012 IEEE International Conference on Robotics and Biomimetics (ROBIO)*, pp. 217–222, IEEE, 2012.

[16] F. Xu, X. Wang, and L. Wang, "Cable inspection robot for cable-stayed bridges: Design, analysis, and application," *Journal of Field Robotics*, vol. 28, no. 3, pp. 441–459, 2011.

[17] W. Song, H. Jiang, T. Wang, D. Ji, and S. Zhu, "Design of permanent magnetic wheel-type adhesion-locomotion system for water-jetting wall-climbing robot," *Advances in Mechanical Engineering*, vol. 10, no. 7, p. 1687814018787378, 2018.

[18] S. T. Nguyen and H. M. La, "Development of a steel bridge climbing robot," in *2019 IEEE/RSJ International Conference on Intelligent Robots and Systems (IROS)*, pp. 1912–1917, IEEE, 2019.

[19] A. Bircher, K. Alexis, M. Burri, P. Oettershagen, S. Omari, T. Mantel, and R. Siegwart, "Structural inspection path planning via iterative viewpoint resampling with application to aerial robotics," in *2015 IEEE International Conference on Robotics and Automation (ICRA)*, pp. 6423–6430, IEEE, 2015.

[20] A. Jimenez-Cano, J. Braga, G. Heredia, and A. Ollero, "Aerial manipulator for structure inspection by contact from the underside," in *2015 IEEE/RSJ international conference on intelligent robots and systems (IROS)*, pp. 1879–1884, IEEE, 2015.

[21] T. Yoshiike, M. Kuroda, R. Ujino, H. Kaneko, H. Higuchi, S. Iwasaki, Y. Kanemoto, M. Asatani, and T. Koshiishi, "Development of experimental legged robot for inspection and disaster response in plants," in *2017 IEEE/RSJ International Conference on Intelligent Robots and Systems (IROS)*, pp. 4869–4876, IEEE, 2017.

[22] M. Hutter, C. Gehring, D. Jud, A. Lauber, C. D. Bellicoso, V. Tsounis, J. Hwangbo, K. Bodie, P. Fankhauser, M. Bloesch, *et al.*, "Anymal-a highly

mobile and dynamic quadrupedal robot," in *2016 IEEE/RSJ International Conference on Intelligent Robots and Systems (IROS)*, pp. 38–44, IEEE, 2016.

[23] S. Kitano, S. Hirose, G. Endo, and E. F. Fukushima, "Development of lightweight sprawling-type quadruped robot titan-xiii and its dynamic walking," in *2013 IEEE/RSJ International Conference on Intelligent Robots and Systems*, pp. 6025–6030, IEEE, 2013.

[24] M. Bjelonic, N. Kottege, T. Homberger, P. Borges, P. Beckerle, and M. Chli, "Weaver: Hexapod robot for autonomous navigation on unstructured terrain," *Journal of Field Robotics*, vol. 35, no. 7, pp. 1063–1079, 2018.

[25] A. Saito, K. Nagayama, K. Ito, T. Oomichi, S. Ashizawa, and F. Matsuno, "Semi-autonomous multi-legged robot with suckers to climb a wall," *Journal of Robotics and Mechatronics*, vol. 30, no. 1, pp. 24–32, 2018.

[26] M. B. Khan, T. Chuthong, C. D. Do, M. Thor, P. Billeschou, J. C. Larsen, and P. Manoonpong, "icrawl: An inchworm-inspired crawling robot," *IEEE Access*, vol. 8, pp. 200655–200668, 2020.

[27] T. Bandyopadhyay, R. Steindl, F. Talbot, N. Kottege, R. Dungavell, B. Wood, J. Barker, K. Hoehn, and A. Elfes, "Magneto: A versatile multi-limbed inspection robot," in *2018 IEEE/RSJ International Conference on Intelligent Robots and Systems (IROS)*, pp. 2253–2260, IEEE, 2018.

[28] P. Kriengkomol, K. Kamiyama, M. Kojima, M. Horade, Y. Mae, and T. Arai, "A new close-loop control method for an inspection robot equipped with electropermanent-magnets," *Journal of Robotics and Mechatronics*, vol. 28, no. 2, pp. 185–193, 2016.

[29] F. Rochat, P. Schoeneich, M. Bonani, S. Magnenat, F. Mondada, H. Bleuler, and C. Hürzeler, "Design of magnetic switchable device (msd) and applications in climbing robot," in *Emerging trends in mobile robotics*, pp. 375–382, World Scientific, 2010.

[30] A. Peidró, M. Tavakoli, J. M. Marín, and Ó. Reinoso, "Design of compact switchable magnetic grippers for the hyrecro structure-climbing robot," *Mechatronics*, vol. 59, pp. 199–212, 2019.

[31] S. Hong, Y. Um, J. Park, and H.-W. Park, "Agile and versatile climbing on ferromagnetic surfaces with a quadrupedal robot," *Science Robotics*, vol. 7, no. 73, p. eadd1017, 2022.

[32] A. Mazumdar and H. H. Asada, "Mag-foot: A steel bridge inspection robot," in *2009 IEEE/RSJ International Conference on Intelligent Robots and Systems*, pp. 1691–1696, IEEE, 2009.

[33] "XL430-W250 Smart servo." https://emanual.robotis.com/docs/en/dxl/x/xl430-w250/.

[34] "Permanent electromagnetic holder. (KEP-3C)." http://kanetec.co.jp/en/pdf/073_082.pdf.

[35] "Spherical Neodymium Magnet NdFeB." https://jp.misumi-ec.com/vona2/detail/221006221635/.

[36] "PQ12-R Micro Linear Servos." https://www.actuonix.com/pq12-30-6-r.

[37] J. C. Romao, M. Tavakoli, C. Viegas, P. Neto, and A. T. de Almeida, "Inchwormclimber: A light-weight biped climbing robot with a switchable magnet adhesion unit," in *2015 IEEE/RSJ International Conference on Intelligent Robots and Systems (IROS)*, pp. 3320–3325, IEEE, 2015.

[38] M. Tavakoli, J. Lourenco, C. Viegas, P. Neto, and A. T. de Almeida, "The hybrid omniclimber robot: wheel based climbing, arm based plane transition, and switchable magnet adhesion," *Mechatronics*, vol. 36, pp. 136–146, 2016.

[39] A. Parness, N. Abcouwer, C. Fuller, N. Wiltsie, J. Nash, and B. Kennedy, "Lemur 3: A limbed climbing robot for extreme terrain mobility in space," in *2017 IEEE International Conference on Robotics and Automation (ICRA)*, pp. 5467–5473, IEEE, 2017.

[40] T. Takubo, T. Arai, K. Inoue, H. Ochi, T. Konishi, T. Tsurutani, Y. Hayashibara, and E. Koyanagi, “Integrated limb mechanism robot asterisk,” *Journal of Robotics and Mechatronics*, vol. 18, no. 2, pp. 203–214, 2006.